Dysregulation of neural activity and microglia function following exposure to the global environmental contaminant perfluorooctane sulfonate (PFOS)

Shannon E. Paquette[1#], Nathan R. Martin[1#], April Rodd[1], Katherine E. Manz[2], Manuel Camarillo[1], Eden Allen[1], Kurt Pennell[2], and Jessica S. Plavicki[1*]

[1]Department of Pathology & Laboratory Medicine, Brown University, Providence, RI

[2]School of Engineering, Brown University, Providence, RI

[#]These authors contributed equally

*Corresponding author

ABSTRACT

Pollution is a driving force in climate change and an important modifier of human health. Humans are chronically exposed to complex chemical mixtures and, correspondingly, researchers are disentangling the contribution of different contaminants to human neuropathologies. Per- and polyfluoroalkyl substances (PFAS) are biopersistent pollutants and, due to their diverse applications, have become global contaminants. Perfluorooctane sulfonate (PFOS), a prevalent PFAS congener, impairs humoral immunity; however, its impact on innate immunity is unclear. Given the critical roles of innate immune cells, namely microglia, in brain development and homeostasis, we asked whether exposure adversely affects microglial function. Herein, we demonstrate developmental PFOS exposure produces microglial activation and upregulation of the microglia activation gene *p2ry12*. PFOS-induced microglial activation heightened microglial responses to brain injury, in the absence of increased cell death or inflammation. Use of the photoconvertible calcium indicator CaMPARI revealed PFOS exposure heightened neural activity, while optogenetic silencing of neurons was sufficient to normalize microglial responses to injury. Exposure to perfluorooctanoic acid, an immunotoxic PFAS, did not alter neuronal activity or microglial behavior, further supporting a role for neural activity as a critical modifier of microglial function. Together, this study reveals how contaminant-induced changes in brain activity can shape brain health.

INTRODUCTION

Pollution poses a global threat to environmental, ecologic, and economic health and stability. As international geologic committees consider whether we have now entered the “Anthropocene Age,” it is of increasing importance to understand the broad impacts of human-made pollutants. It is also worth emphasizing that the burden of pollution is disproportionately shared, with minority and low-income communities being more susceptible to the physical consequences of insufficient regulatory laws, industrial waste disposal, and air pollution (Bullard 1994, Muller, Sampson and Winter 2018, Liu et al. 2021). If we

are to protect our health, society, and environment, more research efforts are needed to address the costs of our past and present environmental negligence.

One major class of chemicals of increasing concern are per- and polyfluoroalkyl substances (PFAS). While PFAS were only introduced in industrial manufacturing in the mid-20th century, the expansive and international utilization of PFAS has led to near universal exposure in humans (Kannan et al. 2004, Paul, Jones and Sweetman 2009). PFAS congeners are found in fire-fighting foams, commercial household products such as water-repellant fabrics, food packaging, and non-stick finishes, and are used in a variety of applications in the aerospace, aviation, and automotive industries (USEPA). Structurally, PFAS consist of fully or polyfluorinated aliphatic substances of varying carbon chain length and head groups, with longer chain length tending to be associated with increased toxicity (Buck et al. 2011, Gomis et al. 2018, Chambers, Hopkins and Richards 2021). The strength of carbon-fluorine bonds lends most PFAS to be biopersistent, bioaccumulative, and resistant to degradation. As such, PFAS have acquired the disconcerting moniker "forever chemicals."

Of the 4,700+ PFAS congeners (OECD 2018), one of the most environmentally prevalent and extensively studied is perfluorooctane sulfonate (PFOS). PFOS has an 8-carbon chain with a sulfonic acid head group and adversely impacts the functioning and health of several major organ systems (Sunderland et al. 2019, Zeng et al. 2019), and is considered a metabolic, endocrine, and immune disruptor (DeWitt, Copeland and Luebke 2009a, DeWitt et al. 2012, DeWitt et al. 2009b, DeWitt et al. 2016, Stein et al. 2016, Braun 2017, Chang et al. 2016). *In utero* and developmental exposure to PFOS has particularly concerning consequences on adaptive immunity. Grandjean et al. demonstrated that elevated PFOS levels in infancy and early childhood significantly attenuate adaptive immune responses, curb antibody production, and limit vaccine efficacy (Grandjean et al. 2012, Grandjean et al. 2017). Such studies reinforce the necessity of understanding the impact of pollution on population health, especially considering the need to vaccinate individuals against emerging or evolving pathogens. PFOS-induced humoral immune suppression (DeWitt et al. 2012, Peden-Adams et al. 2008) prompted the National Toxicology Program to classify PFOS as a "presumed immune hazard to humans" in 2016 (NTP 2016). However, the effects of PFOS on innate

immunity are still largely inconclusive, with some groups finding that PFOS dampens innate cell infiltration, gene expression, or activity (Castano-Ortiz, Jaspers and Waugh 2019, Keil et al. 2008, Ryu et al. 2014), and others describing heightened inflammation or immune function (Dong et al. 2012, Qazi et al. 2009, Wang et al. 2021). Even less understood is the tissue-specific impact of PFOS on local immune populations, namely tissue-resident macrophages. Tissue-resident macrophages are largely yolk-sac or fetal liver-derived, heterogenous, and most notably carry out discrete, non-canonical tissue-specific functions essential for development and homeostasis (Davies et al. 2013). Determining whether tissue-resident macrophages are PFAS targets, especially during development, is essential for our understanding of long-term consequences of macrophage dysregulation following PFAS exposure.

In this work, we focus on microglia, the resident immune population of the central nervous system (CNS), as a potential PFOS target. Beyond effector immune responses, microglia have a highly dynamic and diverse repertoire of homeostatic functions, including developmental pruning of extra-numerary synapses (Paolicelli et al. 2011, Schafer et al. 2012), facilitating synaptogenesis and maturation (Hoshiko et al. 2012), and regulation of neural plasticity and dendritic spine density through frequent synaptic monitoring (Parkhurst et al. 2013, Szepesi et al. 2018, Wake et al. 2009). As sentinels of the CNS, these persistent, self-renewing cells are also highly sensitive and rapidly adaptable to any changes in their environment. As such, microglia are often categorized into two broadly termed polarization states: homeostatic and ramified versus activated and reactive. Homeostatic microglia have highly motile processes that continuously extend and retract to survey the surrounding environment, including active synapses in an activity-dependent manner (Dissing-Olesen et al. 2014, Eyo et al. 2014, Nimmerjahn, Kirchhoff and Helmchen 2005, Tremblay, Lowery and Majewska 2010, Wake et al. 2009). Conversely, activated microglia, which are actuated by pathogenic or local endogenous stimuli, exhibit an amoeboid-like morphology, are migratory, proliferative, phagocytic, and secrete immunomodulatory and neuroactive factors (Kettenmann et al. 2011).

Microglia activation has been well documented in disease models of various neuropathological states, including Down Syndrome (Pinto et al. 2020), Alzheimer's disease (Mancuso et al. 2019), and epilepsy (Hiragi, Ikegaya and Koyama 2018). Due to the critical regulatory roles of microglia in neural health and

development, there has been a concerted effort to clarify the mechanisms of bidirectional cross-talk between neurons and microglia (Szepesi et al. 2018). However, the impact of environmental exposures on neuron-microglia interactions during developmentally sensitive periods of life, including gestation, has been largely overlooked. Some epidemiological studies suggest correlations between developmental PFOS exposure and ADHD incidence, while others found no such relationship (Fei et al. 2008, Lien et al. 2016, Liew et al. 2015, Ode et al. 2014). Meanwhile in mice, a single neonatal PFOS exposure is sufficient to alter proteins required for neuronal growth and synaptogenesis, as well as cause spontaneous behavior and hyperactivity in adults (Johansson, Eriksson and Viberg 2009, Johansson, Fredriksson and Eriksson 2008). Developmental exposure to PFOS was also shown to cause hyperactive locomotor activity in larval zebrafish (Gaballah et al. 2020, Huang et al. 2010, Jantzen, Annunziato and Cooper 2016). *In vitro* experiments using cultured neurons revealed that PFOS interacts with inositol 1,4,5-triphosphate receptors (IP_3Rs) and ryanodine receptors (RyRs), leading to the release of intracellular calcium stores, which suggests a potential role for calcium in PFOS-induced neurotoxicity (Liu et al. 2011). However, it is still not known whether the induced locomotor activity in zebrafish is attributed to neuronal hyperactivity or skeletal muscle calcium utilization (Christou et al. 2020). It is also not known if potential changes in the neuronal environment following PFOS exposure can impact microglia function, and vice versa.

Herein, we employed functional neuroimaging in larval zebrafish to provide the first *in vivo* account of PFOS-induced disruption of neuronal activity. We further observed the direct effects of PFOS-induced neuronal hyperactivity on microglia activation and function by using an established brain injury model for zebrafish (Schmidt et al. 2014). By utilizing optogenetics to independently modulate the neuronal or microglial electrical state, we demonstrate that PFOS-induced neuronal hyperactivity and microglia hyperresponsiveness could be reversed, respectively, further supporting the role of neuronal activity on

110 microglia function. Lastly, by exposing larvae to a non-excitatory PFAS congener, we demonstrate that
111 structurally similar compounds can have significantly distinct effects on CNS health and neural cell function.

112

113 **RESULTS**

114 **PFOS exposure activates microglia and renders them hyperresponsive to minor brain**
115 **injury.**

116 Studies utilizing immortalized microglia cell lines suggest PFOS exposure decreases microglial viability,
117 mitochondrial stability, and increases reactive oxygen species production *in vitro* in a concentration-
118 dependent manner (Ge et al. 2016, Zhang et al. 2011). However, whether PFOS affects microglia activation
119 and function *in vivo* is not yet known. Given the critical developmental and modulatory roles of microglia in
120 the CNS, we sought to determine whether embryonic exposure to PFOS had a direct effect on microglia
121 colonization of the developing brain. We selected a concentration exposure range based on previously
122 published work demonstrating the adverse effects of PFOS exposure on pancreatic development in larval
123 zebrafish (Sant et al. 2017, Chen et al. 2014). Transgenic zebrafish embryos with macrophage-specific
124 GFP expression under the *mpeg1* promoter (*Tg(mpeg1:EGFP)*) (Ellett et al. 2011b) were chronically
125 exposed to either a control solution (0.1% DMSO) or 28 μM PFOS from 4 hours post-fertilization (hpf) until
126 3 days post-fertilization (dpf) (Figure 1A). Using liquid chromatography with high-resolution mass
127 spectrometry (LC-HRMS), we validated our exposure solutions and determined that 28 μM PFOS resulted
128 in a total body burden of 32.22 ± 2.57 ng/embryo at 48 hpf and 70.46 ± 2.72 ng/embryo at 72 hpf (Table 1).
129 Next, we examined microglial number and morphology at 72 hpf, a time point at which no significant
130 increase in mortality was observed across the tested concentration range (Table 2). Non-parenchymal,
131 parenchymal, and total microglia number was not changed at 72 hpf between the control and 28 μM PFOS-
132 exposed larvae (Figure 1—figure supplement 1A-C). While microglia number was unchanged, cell
133 morphology was significantly altered. PFOS-exposed microglia acquired a less ramified and more
134 amoeboid cell shape, resembling an activated phenotype (Figure 1D-E'' vs 1I-J''). This corresponded to a
135 significant reduction in cell area (Figure 1N), cell perimeter (Figure 1O), and the acquisition of a more

circular cell shape as calculated by a decrease in the perimeter-to-area ratio (Figure 1P). Relative mRNA analysis for the gene *p2ry12*, a G-protein coupled receptor directly involved in microglia activation and migration behavior (Badimon et al. 2020, Davalos et al. 2005, Yu et al. 2019), was also significantly upregulated in the brains of PFOS-exposed larvae (Figure 1Q), further supporting the activation of microglia. To determine whether the observed phenotypic changes were accompanied by functional changes, we tested whether pollutant-induced microglia activation affected the ability of microglia to respond to minor brain injury using an established zebrafish injury model (Schmidt et al. 2014, Sieger et al. 2012). At 72 hpf, larvae were injured at the right hemisphere of the telencephalon using a pulled glass needle (OD 9 um; Figure 1B) and microglia recruitment to the injury site was monitored for the first 4.5 hours post-injury (hpi; Figure 1C). PFOS-exposed larvae had a significant increase in microglial recruitment in the first 4.5 hpi compared to sibling controls (Figure 1R; Figure 1—figure supplement videos 1 versus 2). Additionally, the area of microglial response in exposed larvae was significantly expanded at 4 hpi (Figure 1G vs 1L; Figure 1S), which persisted up to 12 hpi (Figure 1H vs 1M; Figure 1T). A major function of microglia following brain injury is the removal of damaged cells and cellular debris to prevent excessive inflammation, which is deleterious to brain health (Donat et al. 2017). Using the nucleic acid stain acridine orange in live larvae, we asked whether an increased incidence of cell death was driving the microglia response to injury in pollutant-exposed larvae; however, PFOS-exposure did not result in an increase in cell death in the whole brain nor at the injury site at 1 or 4 hpi (Figure 1—figure supplement 1D-H). Moreover, relative mRNA expression of the proinflammatory cytokines *il1β*, *tnfα*, and *il6* were unchanged in larval brains following exposure (Figure 1—figure supplement 1I). While these data suggest microglial hyperresponsiveness in PFOS-exposed larvae is not directed by canonical damage signaling, the

157 morphological and transcriptional shift of microglia toward an activated phenotype (Figure 1N-Q) suggest
158 that microglia are activated following PFOS exposure and may be targets of PFOS toxicity.

159 **Optogenetic Reversal of Microglia Activation State Normalizes the Microglial Response to**
160 **Injury**

161 To determine the extent to which microglial activation state contributed to the heightened microglial
162 response to injury, we next asked whether PFOS-induced microglia activation could be reversed *in vivo*,
163 and if this reversal of activation state was sufficient to normalize the injury response. Since the homeostatic
164 microglia membrane potential is largely maintained by chloride channel currents (Newell and Schlichter
165 2005), we utilized transgenic zebrafish expressing the light-gated chloride pump halorhodopsin (eNpHR3.0)
166 specifically in microglia (*Tg(mpeg1:Gal4FF;UAS:eNpHR3.0-mCherry)*) (Figure 2A). This third-generation
167 opsin exhibits reliable membrane trafficking for uniform surface expression, is resistant to inactivation, and
168 has step-like, potent photocurrents that are stable over long timescales (Gradinaru et al. 2010). Larvae with
169 halorhodopsin^{+} microglia were exposed to 28 μM PFOS to induce microglia activation by 72 hpf, at which
170 point the larvae were injured and exposed to 589 nm light for 4 hours (Figure 2B,C). We confirmed the
171 morphological shift toward an activated phenotype in unstimulated PFOS-exposed larvae (Figure 2D-E'')
172 and compared the microglia morphology of unstimulated larvae to larvae stimulated by 589 nm light.
173 Halorhodopsin stimulation of PFOS-exposed microglia produced a significantly more ramified morphology
174 (Figure 2H-I''). Additionally, while stimulation had no effect on microglia area (Figure 2L), it significantly
175 increased the cell perimeter (Figure 2M) and perimeter-to-area ratio (Figure 2N), supporting the transition
176 from amoeboid to ramified. We also confirmed 589 nm stimulation alone had no impact on microglia
177 morphology by stimulating and assessing microglia from PFOS-exposed larvae lacking halorhodopsin
178 expression, *Tg(mpeg1:Gal4FF;UAS:nfsb-mCherry)* (Figure 2—figure supplement 1). We next tested
179 whether optogenetic modulation of microglia activation state was sufficient to rescue their responses to
180 brain injury. Indeed, while unstimulated larvae had exacerbated microglia responses to injury (Figure 2F vs
181 2G), stimulation of halorhodopsin in PFOS-exposed microglia significantly reduced the microglia response
182 (Figure 2G vs 2K; area of response quantified in Figure 2O). These data suggest that modulation of

183 microglia activity state alone is sufficient to normalize their functions following toxicant exposure.
184 Additionally, given that microglia are highly responsive to their microenvironments, it suggests that microglia
185 hyperresponsiveness in PFOS-exposed larvae may be influenced by changes in neuronal communication.

186 **Developmental PFOS exposure alters global and regional neuronal network activity**

187 While evidence suggests PFOS exposure can impact developing and adult brain health, the direct effects
188 of exposure on neuronal network activity, whole brain metabolome, and neurotransmitter release are not
189 well understood. To understand the effect of PFOS on global brain activity *in vivo*, we assessed neuronal
190 calcium activity by driving the fluorescent calcium sensor CaMPARI (Calcium-Modulated Photoactivatable
191 Ratiometric Integrator) under the pan-neuronal promoter *elavl3* (*Tg(elavl3:CaMPARI(W391F+V398L))*^{jf9}).
192 CaMPARI is a permanent photoconvertible calcium sensor that undergoes allosteric chromophore
193 modulation from green-to-red in response to ultraviolet light, but only upon simultaneous binding of free
194 intracellular calcium (Fosque et al. 2015). Therefore, inactive neurons at the time of photoconversion are
195 green, while active neurons convert to red (Figure 3A-D). In this study, free swimming larvae were subjected
196 135 mW/cm^2 of 405 nm light for 1 minute inside our behavioral unit (Figure 3—figure supplement 1A-D).
197 We validated our CaMPARI photoconversion, imaging, and analysis pipeline by exposing larvae to
198 pentylenetetrazol (PTZ), a GABAA receptor antagonist known to cause neuronal hyperactivity and seizures
199 in zebrafish (Baraban et al. 2005) (Figure 3—figure supplement 1E-H versus 1E'-H'). Indeed, 10 mM PTZ
200 led to a significant ratio-metric increase of neuronal intracellular calcium in the optic tectum and cerebellum,
201 as well as the whole brain (Figure 3—figure supplement 1J). To determine whether PFOS exposure
202 affected brain activity, we applied this validated pipeline to 3 dpf larvae exposed to 28 μM PFOS, the same
203 concentration used for the injury model. PFOS exposure caused a notable increase in neuronal activity in
204 the forebrain, optic tectum, and hindbrain, with a significant increase in the cerebellum and whole brain
205 collectively (Figure 3G,I). We also examined whether lower concentrations of PFOS were able to induce
206 changes in neuronal activity. While there were no significant changes in network activity at 3 dpf following
207 7 μM PFOS (Figure 3F,H), this group had significant increases in regional and global activity at 5 dpf (Figure
208 3K,M), as did the 14 μM exposed group (Figure 3L,N). We also assessed gross brain morphology of PFOS-

exposed larvae and found that while whole brain area was slightly reduced at 3 dpf, brain area is unchanged by 5 dpf, suggesting that the effects of PFOS on morphology are nominal and temporary (Figure 3—figure supplement 2). Together, these data reveal that PFOS has a time and concentration dependent effect on network activity, exclusive of effects on gross morphology.

To better understand the neurochemical changes in the PFOS exposed brain, we performed an untargeted metabolome wide association study (MWAS) on isolated heads of 3 dpf control and 28 μM PFOS exposed larvae. Several features were significantly upregulated or downregulated between the control and exposed groups (Figure 3—figure supplement 3A). Significantly changed metabolites from the MWAS were further analyzed for pathway enrichment using MetaboAnalystR (Chong and Xia 2018). Several of the significantly enriched pathways, including glutamate metabolism, aspartate and asparagine metabolism, tyrosine metabolism, and phosphoinositide metabolism, are involved in neuronal excitation, catecholamine synthesis, and neurotransmitter release, uptake, and recycling (Figure 3—figure supplement 3C; Table 3). Together with the CaMPARI analysis, these data suggest the brain is a PFOS target and significant neurochemical imbalances occur following exposure.

We next sought to determine whether the neurochemical imbalances were predictors of abnormal behavioral activity. A single exposure event to PFOS is sufficient to drive spontaneous behavior and hyperactivity in adult mice (Johansson et al. 2008) and can lead to tonic convulsions in response to an ultrasonic stimulus (Sato et al. 2009). Additionally, developmental exposure to PFOS decreases the frequency but increases the intensity of spontaneous locomotor activity in both mice and larval zebrafish in a concentration-dependent manner (Spulber et al. 2014). To first determine whether our exposure paradigm replicates previously reported behavioral hyperactivity, we exposed embryos to either 7 μM, 14 μM, or 28 μM PFOS at 4 hpf, and performed a behavioral photomotor response assay at 3 dpf, 4 dpf, and 5 dpf (Figure 4—figure supplement 1A,B). Consistent with previous locomotor assays at 6 dpf (Gaballah et al. 2020), PFOS-exposed larvae exhibited significantly increased photomotor responses to light changes, designated by increased distance traveled within the well at 3 dpf following 28 μM exposure (Figure 4—figure supplement 1E-H) and 5 dpf following 7 μM and 14 μM exposure (Figure 4—figure supplement 1N-

R). In addition to distanced traveled, behavior videos were analyzed to assess the frequency of center avoidance within the wells of a 24-well plate. Similar to the mammalian open-field test, center avoidance in a well is an indication of zebrafish anxiety, while willingness to cross the center suggests a reduced anxiety level (Colwill and Creton 2011). As such, we examined the time each larva spent along the well's edge (anxious) versus center (exploratory) throughout each photomotor assay (Figure 4 A,B). PFOS exposure resulted in a notable increase in anxiety-like behavior in all dosed groups at 3, 4, and 5 dpf (Figure 4 C-E). Since anxiety, fear, and aversive behaviors are regulated by the medial habenula in zebrafish (Mathuru and Jesuthasan 2013, Okamoto, Agetsuma and Aizawa 2012), we assessed neuron activity at the habenula using CaMPARI. Only 14 µM PFOS exposed larvae showed a significant difference in habenular activity at 3 and 5 dpf (Figure 4—figure supplement 2), suggesting that habenular dysregulation alone may not be an accurate predictor of anxiety in larval zebrafish. Interestingly, while 14 µM PFOS-exposed larvae exhibited the most pronounced anxiety responses at 3, 4, and 5 dpf, they did not have an increase in swim activity at 3 dpf (Figure 4—figure supplement 1H), and only showed an increase in activity when the behavior box light was "On" at 4 dpf (Figure 4—figure supplement 1K). This suggests that anxiety behaviors are separable from swim hyperactivity and support the need to more thoroughly understand the independent behavioral changes associated with PFOS exposure.

Microglia mutants have reduced swim behavior, but are more reactive to light transitions following PFOS exposure Neuron-microglia bi-directional signaling enables the reciprocal regulation of microglia and neuronal functions, including microglial modulation of neuronal activity and circuit refinement (Marinelli et al. 2019, Szepesi et al. 2018). Considering that microglia become activated following PFOS exposure, we sought to determine whether or not PFOS-induced microglial dysfunction during early larval development influenced neuronal excitation and behavior. To do this, we exposed PFOS to zebrafish with a null mutation for *irf8* (*irf8*$^{st96/st96}$), a gene required for macrophage formation during primitive and transient definitive hematopoiesis (Shiau et al. 2015). *irf8* mutant larvae lack the earliest embryonic-derived macrophage populations, including microglia (Shiau et al. 2015). Control *irf8* mutants had a consistent reduction in overall swim behavior and were significantly less reactive to the light-dark transitions (Figure 5A,B). Exposure to 8 µM PFOS significantly increased swim behavior of 5 dpf wildtype and *irf8* mutant

larvae (Figure 5A). However, unlike the control-treated *irf8* mutants, PFOS-exposed mutants were not consistently less active during the photomotor assay. PFOS-exposed mutants also exhibited the most dramatic behavioral response to the light-dark transitions, especially during the second dark cycle (Figure 5B; "First Minute"). In addition, while wildtype control larvae and wildtype PFOS-exposed larvae had a 14.9% and 23.8% reduction in swim activity by the end of the second dark cycle, respectively, PFOS-exposed *irf8* mutants had a 47.6% reduction (Figure 5B). These data suggest that microglia may attempt to modulate the PFOS-exposed brain, such that the absence of microglia may further promote PFOS-induced behavioral reactivity. Heightened reactivity may also result in behaviors that impair swim ability, such as seizing or convulsions. Microglia-deficient larvae with transgenic expression of neuron-driven CaMPARI also had significant increases in regional and global calcium activity over controls, though these were not significant between genotypes (Figure 5C).

Neuronal activity modulates microglia responsiveness

While microglia are not wholly responsible for the behavioral or neuronal phenotypes seen with PFOS-exposure, PFOS-induced neuronal hyperactivity may still be an important modulator of microglia. To test this hypothesis, 3 dpf larvae were treated with 5 mM PTZ to induce neuronal activity, then were injured in the right telencephalon as described. PTZ-induced neuronal hyperactivity significantly increased the microglia response at 4 hpi, similar to that of PFOS-exposed larvae (Figure 6—figure supplement 1). We next asked whether inhibiting neuronal activity using optogenetics could normalize the hyperresponsive microglial phenotype seen with PFOS exposure. Previous studies implementing halorhodopsin for neuronal hyperpolarization in zebrafish demonstrated significant suppression of coiling behavior, swim activity, and silencing of single neuron spiking (Antinucci et al. 2020, Arrenberg, Del Bene and Baier 2009). Larvae expressing *Tg(elavl3:Gal4;cryaa:RFP;UAS:eNpHR3.0;mpeg1:EGFP),* which have pan-neuronal expression of halorhodopsin as well as GFP-labeled macrophages, were exposed to either a control solution or 28 μM PFOS at 4 hpf. After brain injury at 3 dpf, larvae were either left unstimulated or stimulated for 4 hours with 589 nm light to silence neuronal activity. Unstimulated PFOS-exposed larvae exhibited a significant increase in microglia response to injury, as demonstrated earlier (Figure 6E,F,I). Conversely,

neuronal hyperpolarization rescued microglia hyperresponsiveness (Figure 6G,H,I), further supporting that pollutant-induced changes in the neural signaling environment significantly influences microglia behavior, independent of cell death or inflammation.

Exposure to PFOA, an immunotoxic PFAS congener, does not result in microglia hyperresponsiveness

To further assess if microglia hyperresponsiveness following PFOS exposure is a result of neuronal hyperactivity, we exposed larval zebrafish to a structurally similar PFAS congener, perfluorooctanoic acid (PFOA). Whereas PFOS has a sulfonic acid head group, PFOA is an 8-carbon PFAS with a carboxylic acid head group. PFOA has been shown to cause significant health effects, including immunotoxicity, elevated cholesterol, dysregulated liver metabolism, kidney dysfunction, thyroid disease, among many others (Reviewed in (Post, Cohn and Cooper 2012)). Previous reports using larval zebrafish have found that PFOA concentrations ranging from 4.4 μM to 80 μM did not result in a significant change in 6 dpf swim behavior during photomotor response assays (Gaballah et al. 2020). Therefore, we hypothesized that PFOA may also have unchanged neuronal network activity, making it an ideal candidate to address the capacity of neuronal activity to influence microglial function. Following the same exposure paradigm used for PFOS exposure (Figure 1A), zebrafish embryos were dosed with either a control solution (0.1% DMSO) or 64 μM PFOA at 4 hpf. In concordance with previous findings, we found that exposure to 64 μM PFOA did not result in altered swim behavior during photomotor response assays at 5 dpf (Figure 7—figure supplement 1A-D). While PFOA-exposed larvae had shorter body length, there were no observable gross morphological effects on the spine that would affect swimming ability (Figure 7—figure supplement 2). Using neuronally-driven CaMPARI, PFOA exposure did not result in any regional or global changes in neuronal network activity in 5 dpf larvae (Figure 7A-C), unlike the PFOS-exposed groups at this timepoint (Figure 3). Given that PFOA did not result in neuronal hyperactivity, we asked whether PFOA exposure affected microglial responses to brain injury. Indeed, PFOA exposure did not result in altered microglial responses to brain injury (Figure

312 7D-F). Together, these data further support that neuronal hyperactivity is a key driver of microglia response,
313 and that structurally similar PFAS congeners can have distinct impacts on the CNS.

314

315 ## DISCUSSION

316 For more than two decades, researchers have revealed the many biologic, ecologic, and
317 environmental ramifications of PFOS toxicity, as well as the toxicity profiles for a subset of other 'forever
318 chemical' congeners. Here, we used a combination of *in vivo* imaging of cellular behavior, functional
319 neuroimaging, optogenetic modulation, and behavioral assays to address the impact of PFOS exposure on
320 microglia-neuron interactions in larval zebrafish. Our data demonstrate that developmental PFOS exposure
321 activates microglia and induces hyperactivity in response to injury independent of cell death or
322 inflammation. Since the homeostatic microglia membrane potential is largely maintained by chloride
323 channel currents (Newell and Schlichter 2005), we asked whether activating the optogenetic chloride
324 channel halorhodopsin (eNpHR3.0) could rescue microglia hyperresponsiveness. Indeed, electrical
325 modulation of microglia was sufficient to revert microglia from an activated to a homeostatic morphology
326 and normalize their responses to injury, suggesting electrical dysfunction as a previously underappreciated
327 pathway worth interrogating when studying microglial activation and immunotoxicity. PFOS-exposed larvae
328 also exhibited global and regional increases in neuronal activity and anxiety-like behaviors, a previously
329 unidentified neurodevelopmental phenotype of PFOS exposure in zebrafish, with only nominal and
330 temporary impacts on regional brain morphology. We demonstrated that PFOS-induced neuronal
331 hyperactivity was a key mediator of microglia reactivity and that optogenetic silencing of neurons was
332 sufficient to normalize microglia responses to injury. Further, exposure to PFOA did not result in neuronal
333 hyperactivity nor microglia hyperresponsiveness. Together, this study provides the first detailed account of
334 the effects of PFOS exposure on the developing brain *in vivo* and adds neuronal hyperactivity as an
335 important endpoint to assess when studying the impact of toxicant exposures on microglia function.

336 While the immunotoxic impact of PFOS on adaptive immunity has been well documented (DeWitt,
337 Blossom and Schaider 2019), the effects on the innate immune arm are less understood and, at times,
338 contradictory. Studies showing either innate immune activation or suppression following PFOS exposure

339 are likely attributed to varying exposure paradigms, PFOS concentration, animal model, age, or cell line
340 used (Castano-Ortiz et al. 2019, Mollenhauer et al. 2011, Qazi et al. 2009, Ryu et al. 2014, Wang et al.
341 2021). The innate immune system is highly sensitive to both endogenous and xenobiotic stimuli and reacts
342 rapidly, creating a signaling cascade that informs all downstream immune functions (Clark and Kupper
343 2005). Macrophages in particular have the ability to dynamically polarize from a homeostatic state to be
344 pro- or anti-inflammatory depending on the environmental needs. As antigen-presenting cells,
345 macrophages also have the vital role of instructing adaptive immune cells on their responses (Clark and
346 Kupper 2005). The dependency of the adaptive immune system on the innate emphasizes the need to
347 clarify the immunotoxic mechanisms of pollutants like PFOS.

348 This work constitutes the first *in vivo* analysis of microglia, the resident innate immune population
349 of the CNS, following PFAS exposure. Previous *in vitro* studies using immortalized microglia cell lines
350 suggest PFOS exposure decreases microglial viability, mitochondrial stability, and increases ROS
351 production *in vitro* in a concentration-dependent manner (Ge et al. 2016, Zhang et al. 2011). We found that
352 PFOS exposure activates microglia, demonstrated by their morphological transition from ramified to
353 amoeboid shaped, as well as by the upregulation of the microglia activation gene *p2ry12*. P2ry12 is also a
354 purinergic receptor that responds to ATP. It has been demonstrated that microglia response to injury is
355 mediated by glutamate-evoked calcium waves and ATP release from the injury site (Sieger et al. 2012);
356 therefore ATP released by the injury site and/or through high neuronal activity could be contributing to the
357 microglial hyperresponsiveness in PFOS-exposed larvae. It is likewise still unclear to what extent PFOS is
358 acting directly on the microglia or indirectly through neuronal activation. Microglia activation and injury
359 responses were attenuated by both microglia and neuronal optogenetic silencing, suggesting that the
360 neuronal environment has a significant influence on the microglia. While we are providing the first
361 demonstration of microglia activation in response to toxicant exposure, microglia activation has been well
362 documented in disease models of various neuropathological states. In addition, pharmacological prevention
363 of microglia activation or microglia depletion has led to cognitive and functional improvements in some
364 neurological disease models (Goldfarb et al. 2021, Mancuso et al. 2019, Pinto et al. 2020). However, it is
365 worth noting that activated microglia are not inherently pathological. For example, microglia depletion

following stroke significantly increased infarct size, neuronal cell death, and caused calcium overload (Szalay et al. 2016). Microglia depletion during acute seizures also exacerbated excitotoxicity and seizure sensitivity (Liu et al. 2020). Additionally, the regional specificity of microglia activation in a mouse model of chronic stress was considered a protective and/or adaptive response (Tynan et al. 2010).

Due to the developmental and homeostatic roles microglia have on maintaining the excitatory/inhibitory balance (Henstridge, Tzioras and Paolicelli 2019), as well as the situation-specific adverse effects that microglia activation may have on the CNS, we asked whether aberrant microglial activation following PFOS exposure was contributing to the behavioral or neuronal hyperactivity. Using microglia-deficient zebrafish with a mutation in the gene *irf8*, we found that control-treated *irf8* mutants had a consistent reduction in swim behavior that was not seen the PFOS-treated mutants. Additionally, PFOS-exposed mutants had the greatest response to the light-dark transition, suggesting that microglia may actually attempt to repress PFOS-induced behavioral hyperactivity. While microglia loss did not affect baseline neuronal calcium signaling, it is worth noting that microglia loss is distinct from microglia dysfunction, and thus does not rule out the contribution of microglia to neuronal hyperactivity in this context. In addition, microglia increasingly accumulate in synaptic regions between 7 and 28 dpf in zebrafish (Silva et al. 2021), suggesting that any significant death-dependent or activity-dependent neuronal pruning may occur developmentally later than the timepoints investigated in this study. Lastly, the concentrations of PFOS used in this study might increase neuronal activity too substantially or even irreversibly, such that electrical modulation or loss of microglia was not sufficient to influence the activity in a measurable way.

To our knowledge, this is the first report of *in vivo* neuronal hyperactivity caused by embryonic PFOS exposure. We show that embryonic PFOS exposure increased intracellular calcium concentrations across multiple brain regions at various concentrations (7 μM, 14 μM, and 28 μM) and time points (3 dpf & 5 dpf). Both gestational and adult PFOS exposures impact calcium dependent signaling molecules important for memory, including Ca^{2+}/calmodulin dependent kinase II (CaMKII) and cAMP response element-binding protein (CREB) in rats (Liu et al. 2010), suggesting that disrupted calcium signaling is an important mediator of PFOS-induced neurotoxicity. *In vitro* studies also link PFOS toxicity to disrupted calcium homeostasis (Liao et al. 2008, Liu et al. 2011). While the underlying mechanisms remain unknown,

393 possible explanations include increased influx through activation of L-type Ca^{2+} channels (Liao et al. 2008)
394 and release of intracellular calcium stores through interaction with ryanodine and inositol 1,4,5-
395 trisphosphate receptors (Liu et al. 2011). Intracellular calcium excess in neurons promotes excitotoxicity
396 and can cause brain damage leading to various neurological and neurodegenerative disorders (Armada-
397 Moreira et al. 2020, Olloquequi et al. 2018), emphasizing the need to further understand the influence of
398 PFAS on neuronal function. PFAS compounds have also been shown to activate peroxisome proliferator-
399 activated receptors (PPARs) *in vitro* as well as in zebrafish (Rosen et al. 2017, Takacs and Abbott 2007).
400 PPAR-γ in particular is expressed in neurons, microglia, and astrocytes and mediates inflammatory
401 responses in the CNS (Reviewed in (Villapol 2018)). Interrogating PPAR activation in the CNS following
402 PFOS exposure could also provide important information about the specific pathways impacted by
403 exposure.

404 The susceptibility of the developing human brain to PFOS remains a contentious point due to
405 conflicting data. While some studies have demonstrated significant correlations between developmental
406 PFOS exposure and ADHD incidence (Hoffman et al. 2010, Lenters et al. 2019), others found no such
407 relationship (Fei et al. 2008, Lien et al. 2016, Liew et al. 2015, Ode et al. 2014). In the mouse brain, PFOS
408 concentrations have been shown to increase over time and lead to tonic convulsions, despite a lack of
409 morphological phenotypes (Sato et al. 2009). The increase in regional and global network activity
410 demonstrated in this study warrant an assessment of convulsive phenotypes and seizure activity. While
411 outside the scope of this study, determining the threshold and timescale at which neuronal hyperactivity
412 increases incidence of convulsion would be an interesting to pursue

413 Similar to previous reports (Gaballah et al. 2020, Jantzen et al. 2016, Huang et al. 2010), we
414 observed hyperactive swim behavior in PFOS-exposed larvae during photomotor response assays.
415 However, we are the first to report PFOS-induced hyperactivity during the light and dark phases prior to 6
416 dpf. Hyperactive behavioral changes corresponded well with increased intracellular neuronal calcium
417 concentrations. Of note, increased anxiety-like behaviors were separable from increased swim activity at
418 3dpf. This suggests that there may be further disruptions in neuronal communication beyond just increased
419 calcium concentrations influencing swim activity. In-depth regional brain activity analyses, possibly through

420 the integration of developed analytical pipelines (Randlett et al. 2015), could provide further insight into how
421 PFOS induced neural activation is linked to behavioral abnormalities in the larval zebrafish.

422 We identify increased anxiety-like behaviors as a novel phenotype of PFOS neurotoxicity in the
423 larval zebrafish using an adapted open-field test model (Kalueff and Stewart 2012, Ahmad and Richardson
424 2013, Richendrfer et al. 2012). Anxiety is an associated symptom of several neurobehavioral disorders
425 linked to PFAS exposures, including autism spectrum disorder and ADHD (Ode et al. 2014, Skogheim et
426 al. 2021, Oh et al. 2021, Shin et al. 2020). PFOS-induced center avoidance has been observed in mice
427 exposed during adulthood (Fuentes et al. 2007), but developmental anxiety has not been previously
428 reported. Of note, previous published research reporting PFOS-induced larval hyperactivity utilized 96-well
429 plates for higher throughput (Jantzen et al. 2016, Gaballah et al. 2020); however, smaller well sizes may
430 not be conducive to conducting anxiety-like behavioral analyses. We therefore conducted behavioral
431 experiments using 24-well plates, which allowed us to define regions within the well to quantify where fish
432 spent their time swimming. Because dysregulation of habenular activity has been associated with increased
433 anxiety, depression, and fear across species, including the zebrafish (Browne, Hammack and Lucki 2018,
434 Mathuru and Jesuthasan 2013, Okamoto et al. 2012), we assessed whether neuronal calcium was affected
435 in the habenula following PFOS exposure. While only the 14 μM PFOS group showed neuronal
436 dysregulation at the habenula, all groups displayed anxiety like behaviors. This suggests that the habenula
437 may be but one region dictating anxiety-like responses in larval zebrafish, and/or that global neuronal
438 excitation is enough to trigger anxiety responses independent of habenular activity.

439 Not only does this study provide the first *in vivo* assessment of neuronal calcium activity following
440 PFOS exposure, but it is also the first to evaluate PFOA exposure in this context. The chemical structure
441 of PFOA is very similar to PFOS, differing only by the presence of a carboxylic acid head group rather than
442 sulfonic acid, respectively. At the concentrations and timepoints tested, PFOA exposure did not result in
443 increased larval swim behavior or neuronal network activity. However, others have reported that 5 dpf
444 larvae exposed to 1 μM PFOA (Rericha et al. 2021) as well as 14 dpf larvae exposed to 2 μM PFOA
445 (Jantzen et al. 2016) did result in swim hyperactivity. In addition, while neonatal exposure to PFOA in mice
446 has been shown to result in abnormal expression of proteins important for brain growth and neuron function

(Johansson et al. 2009), PFOA exposure of rat primary cortical neurons did not affect spontaneous neuronal activity or burst duration (Tukker et al. 2020). Further analysis is needed to clarify the extent by which PFOA, and other shorter chain length or carboxylic group PFAS congeners, could be neurotoxic or contribute to neural dysregulation. Nevertheless, that PFOA-exposed larvae had normal microglia responses to injury, compared to those exposed to PFOS, highlights the role of neuronal activity on microglia function.

This study provides the first *in vivo* analysis of how developmental PFOS exposure disrupts larval brain health and function. It also highlights the relevance of understanding pollution-induced effects on innate immune cells, in both a non-canonical developmental and homeostatic context, as well as considering the long-term consequences of potential antigen-presentation dysfunction. In summary, the complexity of neural cell communication, especially during the sensitive period of brain development, emphasizes the importance of studying pollutant exposure in non-isolated systems.

MATERIALS & METHODS

Zebrafish husbandry

Zebrafish (*Danio rerio*) maintenance and experimental procedures were approved by the Brown University Institutional Animal Care and Use Committee (IACUC; 19-12-0003) adhering to the National Institute of Health's "Guide for the Care and Use of Laboratory Animals." Zebrafish colonies were maintained in an aquatic housing system (Aquaneering Inc., San Diego, CA) maintaining water temperature (28.5 ± 2°C), filtration, and purification, automatic pH and conductivity stabilization, and ultraviolet (UV) irradiation disinfection. Adult and larval zebrafish were sustained in a 14:10 hour light-dark cycle (Westerfield 2000).

Adult zebrafish were placed into 1.7 L sloped spawning tanks (Techniplast, USA) 15-18 hours prior to mating. Sexes were separated by a transparent partition. Within 2 hours of light cycle onset, the partition was removed, and zebrafish were allowed to spawn for 1 hour. Embryos were collected in fresh egg water (60 mg/L Instant Ocean Sea Salts; Aquarium Systems, Mentor, OH) and placed into 100 mm non-treated

474 culture petri dishes (CytoOne, Cat. No. CC7672-3394) until time of toxicant exposure. Embryonic and larval
475 zebrafish were maintained at 28.5 ± 1°C in an incubator (Powers Scientific Inc., Pipersville, PA) up to 120
476 hours post-fertilization (hpf).
477
478 **Zebrafish lines**
479 The following zebrafish lines were used in this study, either independently or in combination:
480 *Tg(mpeg1:EGFP)* (Ellett et al. 2011b); *Tg(UAS:eNpHR3.0-mCherry)* (Arrenberg et al. 2009, Gradinaru et
481 al. 2010); *Tg*(*elavl3:CaMPARI(W391F+V398L))*^{jf9}) (Fosque et al. 2015); *Tg(elavl3:Gal4-VP16)* (Kimura,
482 Satou and Higashijima 2008); *Tg(mpeg1:Gal4FF)*^{gl25} (Ellett et al. 2011a); *Tg(HuC:Kaede)* (Sato, Takahoko
483 and Okamoto 2006); *Tg(UAS:nfsB-mCherry)* (Davison et al. 2007); *irf8* mutant (TALE-NT 2.0; st96 allele)
484 (Shiau et al. 2015).
485
486 **Perfluorooctanesulfoinc Acid (PFOS) and Perfluorooctanoic Acid (PFOA) exposure**
487 Perfluorooctanesulfonic acid (Sigma-Aldrich, Cat. No. A-5040) and Perfluorooctanoic acid (Sigma-Aldrich,
488 Cat. No. 171468) were prepared by dissolving the powdered compounds in 100% DMSO. PFOS stock
489 concentrations were verified using a LC-HRMS (Table 1) (method details provided below). PFOS stock
490 solution was diluted by a factor of 5000x in a mixture 1:1 methanol:water and 2 mM ammonium acetate to
491 accommodate the detection range of the LC-HRMS. LC/MS grade water and methanol were purchased
492 from Honeywell (Muskegon, MI 49442). Ammonium acetate solution (5 M) was purchased from Millipore
493 Sigma (Burlington, MA 01803).
494
495 Timed spawns of relevant transgenic zebrafish crosses were performed for 1 hr. Embryos were collected
496 and screened for embryo quality at 4 hpf. Healthy embryos were placed in 24-well plates at a density of 3
497 embryos per well. Prior to treatment, PFAS compounds were diluted in egg water to the final concentration
498 of interest. Egg water containing 0.1% DMSO was used as vehicle control. Embryos were dosed with 2 mL
499 of diluted PFOS solution or vehicle control at 4 hpf. The 24-well plates were sealed with parafilm to limit

evaporative loss and placed in an incubator (28.5 ± 1°C). Embryos were dechorionated at 24 hpf and statically exposed until the experimental timepoint of interest.

Brain injury model

At 72 hpf, larval zebrafish were anesthetized in 0.02% tricaine-s solution (Syndel, Ferndale, WA) and restrained dorsal-side-up in 2% agarose (Fisher Scientific, Cat. No. BP160-100). Larvae were injured anteriorly at the right telencephalon with a 9 um OD pulled glass capillary needle. This method was an adaptation for larval fish (Kishimoto, Shimizu and Sawamoto 2012). For time-lapse imaging, larvae were immediately mounted dorsally on a 35 mm glass bottom microwell dish (MatTek, Part No. P35G-1.5-14-C) in 2% low-melting agarose (Fisher Scientific, Cat. No. BP160-100) surrounded by egg water. Multi-slice projection images of the forebrain and optic tectum at various timepoints post-injury, as well as time-lapse videos composed of 10-minute imaging intervals, were captured using a Zeiss LSM 880 confocal microscope at 20x magnification. Area of microglia response was measured using Zen Blue (Zeiss).

Microglial cell quantification

Adult transgenic zebrafish expressing *Tg(HuC:Kaede)* and *Tg(mpeg1:EGFP)* were crossed to generate *Tg(HuC:Kaede; mpeg1:EGFP)* fish, which had pan-neuronal expression of the photoconvertible protein kaede as well as green macrophages. Embryos were exposed to PFOS as described. At 3 dpf, larvae were fixed in 4% paraformaldehyde (PFA, Sigma-Aldrich, Cat. No. P6148) for 18-24 hours at 4°C. Post-fixation, larvae were washed 3 times in PBS-T (phosphate buffered solution + 0.6% Triton-X 100) (Sigma-Aldrich, Cat. No. X100). PBS-T was removed and VECTASHIELD Mounting Media (Vector Labs, Cat. No. H-1000) was added to the samples. Samples incubated for 5 minutes at room temperature, then were gently mixed and placed in -20°C until imaging. The larvae were removed from VECTASHIELD and mounted in 2% low-melting agarose (Fisher Scientific, Cat. No. BP160-100) in 35mm glass bottom microwell dishes (MatTek, Part No. P35G-1.5-14-C). Prior to image acquisition, the kaede fluorophore was photoconverted from green to red fluorescence using 405 nm light (about 1-minute exposure) on the Zeiss LSM 880 confocal microscope. Microglia were defined as macrophages (mpeg1+ cells) amongst and in contact with

differentiated neurons (HuC+ cells) in the forebrain, optic tectum, and hindbrain. The entirety of the zebrafish brains were imaged at 20x magnification (2 tile panels with 10% overlap). Microglia were counted by panning through confocal z-stacks using FIJI/ImageJ. Immune cells in contact with HuC+ differentiated neurons were counted as a parenchymal cells (i.e. microglia). Surface cells in contact with differentiated neurons that failed to extend into the parenchyma were defined as non-parenchymal cells (i.e. macrophage). Location and proximity of mpeg1+ cells were confirmed using z-stack orthogonal views. Each treatment group was compared to controls (0.1 % DMSO) using a One-way ANOVA in GraphPad Prism (Dotmatics, San Diego, CA).

Microglial morphology quantification following PFOS exposure

Microglial morphology was performed on high-resolution confocal micrographs of the optic tectum in fixed transgenic zebrafish larvae expressing either *Tg(mpeg1:EGFP), Tg(mpeg1:Gal4FF;UAS:eNpHR3.0-mCherry),* or *Tg(mpeg1:GalFF;UAS:nfsb-mCherry).* Individual microglia were isolated based on their specific z-stack range, to prevent analysis of overlapping cells, using FIJI/ImageJ. Z-slices were also processed to rescale intensity (compensating for loss of intensity in deeper tissue) and modestly smoothened using Gaussian blur with a sigma radius of 1 to better define cellular extensions and reduce signal noise. Each cell was individually outlined, and morphological parameters measured with CellProfiler software (version 3.1.9) or FIJI/ImageJ. Area, perimeter, and cell shape (perimeter-to-area ratio) were quantified. Unpaired t-tests with Welch's correction were used to evaluate statistical significance using GraphPad Prism (Dotmatics, San Diego, CA).

Quantitative RT-PCR

Larval zebrafish heads were collected at 3 dpf. To collect, larvae were placed on ice for 4 minutes to immobilize swim activity but prevent pain or distress during collection (Wallace et al. 2018). The heads were removed by cutting at the base of the hindbrain at a 45° angle, limiting collection of the heart and pericardium. Heads were pooled (n = 10) and flash frozen in liquid nitrogen. RNA isolation and purification was carried out using the RNeasy Plus Kit (QIAGEN). cDNA synthesis was achieved using the SuperScript

554 IV Reverse Transcriptase First-Strand Synthesis System kit (Invitrogen, Cat. No. 18091050). qRT-PCR for
555 genes of interest was performed with 7.5 ng/uL of cDNA using the ViiA7 Real Time PCR System (Applied
556 Biosystems). Gene targets were detected by using either pre-designed TaqMan probes (Thermo Fisher
557 Scientific) or custom primers with Power Track SYBR Green Master Mix (Thermo Fisher, Cat. No. A46012).
558 See list of probes and primers for qRT-PCR and genotyping below.

Gene	TaqMan ID or Primer Sequences
il6 (m17)	Dr03098117_g1
il1b	Dr03114368_m1
tnfa	Dr03126850_m1
actb1 (b-actin)	Dr03432610_m1
pr2y12	F: 5'-CTTCAGGTCGTCGCTGTTTA-3' R: 5'-AGTGCGTTTCCCTGTTGAT-3'
b-actin	F: 5'-CGAGCAGGAGATGGGAACC-3' R: 5'-CAACGGAAACGCTCATTGC-3'

559

560 **Genotyping *irf8* mutants**

561 *irf8*$^{st96/st96}$ were generated by Shiau et al. via TALEN-targeting (Shiau et al. 2015). After swim behavior
562 testing or CaMPARI imaging, whole larvae were placed in DNA lysis buffer to be used for genotyping. The
563 *irf8* exon 1 fragment was amplified using the following primers: 5'-ACATAAGGCGTAGAGATTGGACG-3'
564 and 5'- GGATGAGGACCGCACTATGTTTC-3'. As this *irf8* mutant has a frameshift mutation at an AvaI site,
565 the PCR product was used for restriction digest with AvaI (New England BioLabs, Cat. No. R0152L) to
566 identify the presence of the mutation.

567

568 **Acridine orange stain**

569 Cell death was determined using the vital dye acridine orange (AO) in live zebrafish embryos. AO is a cell
570 permeable stain that selectively intercalates uncoiled nucleic acid present in apoptotic cells (Delic et al.
571 1991). Zebrafish embryos were injured at 72 hpf and placed in 5 ug/mL acridine orange (ThermoFisher,
572 Cat. No. A1301) diluted in egg water for 20 minutes. Zebrafish were then washed in egg water for 15
573 minutes, refreshing the solution every 5 minutes. Live zebrafish were immediately imaged on a Zeiss LSM
574 880 confocal microscope. For 1 hour-post injury (hpi) analysis, staining took place from 40 minutes to 1 hpi.
575 For 4 hpi analysis, staining took place from 3 hours and 40 minutes to 4 hpi.

576

577 **CaMPARI Photoconversion and Image Acquisition**

578 *Tg[elavl3:CaMPARI(W391F+V398L)]jf9* embryos were screened and the brightest (highest expressing)
579 were selected for toxicant exposure and subsequent photoconversion. Individual embryos were placed into
580 a modified 1-well dish (15 mm diameter) containing PFOS or 0.1% DMSO. The dish was placed onto a
581 constructed pedestal within a DanioVision Observation Chamber (Noldus, Wageningen, The Netherlands)
582 adapted with optogenetics components (Prizmatix, Southland, MI). Use of the pedestal decreased working
583 distance from the LED light source to the free-swimming larva, concordantly increasing light intensity. Cells
584 expressing CaMPARI with high calcium content will photoconvert (green-to-red) in the presence of 405 nm
585 light. Photoconversion was performed by exposing zebrafish to 405 nm (135 mW/cm^2) wavelength light for
586 1 minute. Live zebrafish larvae were then anesthetized in 0.02% tricaine-s (MS-222) and mounted in 2%
587 low-melting agarose in 35mm glass bottom microwell dishes. Confocal z-stacks were acquired on a Zeiss
588 LSM 880 confocal microscope and maximum intensity projections generated in Zen Black (Zeiss)
589 representing a global snapshot of neural activity. Image parameters were set during acquisition of the first
590 image and maintained for the duration of each experiment.

591 **CaMPARI analyses (R/G ratio calculations)**

592 CaMPARI photoconversion from green-to-red during exposure to 405 nm wavelength light was used to
593 determine neuronal calcium levels following PFOS exposure. To assess the level of photoconversion,
594 maximum intensity projections were imported into FIJI/ImageJ. Brain regions of interest including forebrain
595 (FB), habenula (H), optic tectum (OT), cerebellum (Ce), hindbrain (HB), and whole brain (WB) were
596 manually selected and integrated density of red and green was measured. Measurements were blank
597 corrected by selecting 3 separate background regions of each image (Equation 1). The ratios of corrected
598 integrated density were then used to determine R/G ratio for each respective image (Equation 2). R/G ratios
599 were then normalized to the average control R/G ratio within a particular experiment (Equation 3). Unpaired
600 t-tests with Welch's correction were performed on the normalized R/G ratios to determine difference
601 between PFOS treated and control groups.

602 Equation 1: Corrected Integrated Density

603 b = background integrated density

604 d = integrated density of region of interest

605 Corrected Integrated Density (c) = $d - (\Sigma(b1 + b2 + b3)) \div 3$

606

607 Equation 2: R/G Ratio

608 R/G Ratio (r) = $CRed \div CGreen$

609

610 Equation 3: Normalized R/G Ratio

611 $\underline{X}$= mean of control R/G ratios (for each experimental day)

612 Normalized R/G Ratio = $r \div \underline{X}$

613 **Pentylenetetrazol (PTZ) Exposure**

614 For validation of CaMPARI functionality, 3 dpf *Tg(elavl3:CaMPARI(W391F+V398L))*^{jf9} larvae were exposed
615 to 10 mM pentylenetetrazol (PTZ) for 10 minutes. PTZ was washed out 3 times with egg water immediately
616 followed by CaMPARI photoconversion, as described. For assessment of microglia response to injury
617 following PTZ exposure, larvae were exposed to control solution, 28 μM PFOS, or 5 mM PTZ at 72 hpf.
618 Larvae were injured in the right telencephalon, as described, and placed back in their original dosing
619 solutions for 4 hours. At 4 hpi, multi-slice projection images of the forebrain and optic tectum were captured
620 using a Zeiss LSM 880 confocal microscope at 20x magnification. Area of microglia response was
621 measured using Zen Blue (Zeiss). Statistics were performed using unpaired t-tests with Welch's correction
622 using GraphPad Prism (Dotmatics, San Diego, CA).

623

624 **Photomotor Behavioral Response**

625 Behavioral assessments were performed in 24-well plates (ThermoFisher, Cat. No. 144530) using a
626 DanioVision Observation Chamber with EthoVision XT live-tracking software (Noldus, Wageningen, The
627 Netherlands). Larval zebrafish were transferred into individual wells of the same dosing solution

628 approximately 18-24 hours prior to behavioral assessment. All photomotor response assays were
629 performed between 8 AM and 12 PM to prevent behavioral changes attributable to circadian differences.
630 Briefly, zebrafish were placed into the DanioVision observation chamber and acclimated during a 15-minute
631 dark cycle, followed by a 5-minute light cycle (Light 1), a 5-minute dark cycle (Dark 1), another 5-minute
632 light cycle (Light 2), and completed with a 15-minute dark cycle (Dark 2). Behavioral experiments lasted a
633 total of 45 minutes.
634
635 Total distance moved (mm) during light/dark cycles was quantified using the EthoVision XT software as a
636 measure for hyperactivity. Anxiety following PFOS exposure was assessed by monitoring larval well
637 location (center vs. edge) during experimentation. Defined center and edge regions each constituted 50%
638 of total well area. Edge versus center preference was quantified using EthoVision XT. Anxiety data was
639 normalized relative to controls for each experimental replicate. Statistical analyses were performed using
640 GraphPad Prism (Dotmatics, San Diego, CA).
641
642 **Optogenetic Manipulation in Noldus Behavioral Unit**
643 To stimulate the optogenetic channel halorhodopsin in the transgenic lines *Tg(elavl3:Gal4;UAS:eNpHR3.0-*
644 *mCherry)* and *Tg(mpeg1:Gal4ff;UAS:eNpHR3.0-mCherry),* screened larvae were placed a DanioVision
645 observation chamber (Noldus, Wageningen, The Netherlands) outfitted with a 570 nm wavelength laser
646 (Prizmatix, Southland, MI). Halorhodopsin^{+} neurons or microglia were stimulated with 570 nm light for 4
647 hours then immediately imaged for cell morphology or injury response.
648
649 **Targeted Analysis of PFOS Using Liquid Chromatography High Resolution Mass Spectrometry**
650 Chemicals: Certified PFOS and isotope labelled reference standards were purchased from Waters (Milford,
651 MA 01757). LC/MS grade water and methanol were purchased from Honeywell (Muskegon, MI 49442).
652 Ammonium acetate solution (5 M) was purchased from Millipore Sigma (Burlington, MA 01803).
653 Sample Extraction: Larvae were stored in -80°C freezer until extracted and defrosted at 20°C. 1 mL
654 methanol was added to the centrifuge tube containing the embryos. The samples were sonicated for 90

minutes, vortex mixed 1 minute, and allowed to reach equilibrium for 3 hours at 20°C. Samples were then centrifuged at 3,000 rpm for 10 minutes. The following was added to an LC analysis vial: 50 µL of the methanol extract, 10 µL labelled PFOS internal standard, and 440 µL of a mixture containing 1:1 methanol:water and 2 mM ammonium acetate.

Targeted analysis of PFOS was performed using a Thermo Liquid Chromatography (LC) Orbitrap Q Exactive HF-X mass spectrometer (MS) equipped with a Thermo Vanquish UHPLC system. Mobile phase A contained 2 mM ammonium acetate in water and mobile phase B contained 2 mM ammonium acetate in methanol. 20 µl of each sample extract was injected in triplicate and separated in a Thermo Hypersil Gold Vanquish C18 column (50 mm X 2.1 mm x 1.9 µm) at a constant temperature of 60°C. PFOS was eluted from the column at a constant flow rate of 0.4 mL/min using a mobile phase gradient as follows: equilibration with 10% B for 1 minute, followed by a gradient ramp from 10% B to 95% B over 4 minutes and held for 2 minutes, and back to 10 % B over 1 minute and held for 2 minutes (total run time 9 minutes, data collected from 0.6 to 8.5 minutes. The MS was operated in full scan dd-MS^2 mode (70 NCE) with an inclusion list for PFOS. Ionization was performed in negative mode with an ionization window of 1.0 m/z, sheath gas flow rate of 40, auxiliary gas flow rate of 10, sweep gas flow rate of 2, spray voltage of 2.7 kV, 310°C capillary temperature, funnel RF level of 35, and 320°C auxiliary gas heater temperature. Ions were further fragmented in the HCD collision cell filled with N2 (produced by a Peak Scientific Nitrogen Generator, Genius NM32LA). For the full-scan, the Orbitrap was operated with a resolution of 120,000, automatic gain control (AGC) of 3e6, and maximum dwell time of 100ms. For dd-MS2, the Orbitrap was operated with a resolution of 15,000, AGC of 2e5, and maximum dwell time of 400ms.

Four ions were monitored for PFOS, including 498.9302 m/z (quantifying), 79.9573 m/z (confirming), 98.9556 m/z (confirming), and 82.9607 m/z (confirming). The retention time of PFOS was 5.18 min. Quantification was performed in TraceFinder 5.0 General with external seven-point calibration curve prepared by serial dilutions of the calibration standard. Limits of detection (LOD) were determined by injecting a calibration 7 standard seven times and using Equation 4:

682 Equation 4: Limits of Detection (LOD) Calculation

683 LOD=(3*s)/m

684 where s is the sample standard deviation and m is the calibration curve slope. The resulting PFOS LOD
685 was 33.87 ppt.

686

687 **Untargeted Metabolome Wide Association Study**

688 High resolution metabolomics: The sample extracts were re-analyzed using LC-HRMS to collect untargeted
689 metabolomics data. A 10 µL volume was injected in triplicate onto on the Thermo LC-Orbitrap system
690 described above. Two chromatography separation methods were used, normal and reverse-phase. The
691 normal-phase LC was performed with a HILIC column (Thermo Syncronis HILIC 50 mm X 2.1 mm x 3 µm)
692 at a constant temperature of 25ºC. Mobile phase A contained 2 mM ammonium acetate in acetonitrile and
693 mobile phase B contained 2 mM aqueous ammonium acetate. Metabolites were eluted from the column at
694 a constant flow rate of 0.2 mL/minute using a solvent gradient as follows: equilibrate with 10% B for 1
695 minute, increase to 65% B for 9 minutes and hold for 3 minutes, decrease to 10% over 1 minute and hold
696 for 1 minute. The reverse-phase LC was performed with a C18 column (Thermo Hypersil Gold Vanquish,
697 50 mm X 2.1 mm x 1.9 µm) at a constant temperature of 60ºC. Mobile phase A contained 2 mM aqueous
698 ammonium acetate and mobile phase B contained 2 mM ammonium acetate in acetonitrile. Metabolites
699 were eluted from the column at a constant flow rate of 0.5 mL/minute using a mobile phase gradient as
700 follows: equilibration with 2.5% B for 1 minute, increase to 100% B over 11 minutes and held for 2 minutes,
701 and back to 2.5% B over 1 minute and held for 1.5 minutes (total run time 16.5 minutes, data were collected
702 from 0.05 to 12.5 minutes). For both normal and reverse-phase LC, the MS was operated in full scan mode
703 with 120,000 resolution, automatic gain control of 3×10^6, and maximum dwell time of 100 ms. Electrospray
704 ionization was conducted in positive mode for normal-phase and negative mode for reverse phase LC.
705 Ionization was performed at a sheath gas flow of 40 units, auxiliary gas flow of 10 units, sweep gas flow of
706 2 units, spray voltage of 3.5 kV, 310ºC capillary temperature, funnel radio frequency (RF) level of 35, and
707 320ºC auxiliary gas heater temperature.

708

709 Metabolomics data analysis: Data files were converted from *.raw files to *.cdf files using XCalibur file
710 Converter, and then processed in R packages apLCMS (Yu et al. 2009) and xMSanalyzer (Uppal et al.
711 2013) to produce m/z feature tables. Feature intensities were normalized by log2 transformation.
712 Association of metabolite feature with PFOS exposure was assessed using a t-test ($P < 0.05$) in comparison
713 to the control samples. The *P*-values were adjusted using Benjamini and Hochberg with a false discovery
714 rate (FDR) ≤ 20% to control for Type I errors in multiple comparisons. Significant metabolites were analyzed
715 for pathway enrichment using MetaboAnalystR (Chong and Xia 2018) using the zebrafish mummichog
716 curated model, which includes the KEGG, BiGG, and Edinburgh maps. All metabolomics data analysis was
717 performed in R (version 4.0.2).
718
719 **Statistical analyses and reproducibility**
720 As noted in the Methods, control, PFOS, and PFOA stock solutions were validated. Each experiment was
721 carried out in at least three independent experimental replicates. An experimental replicate was considered
722 a cohort of zebrafish that were spawned on separate days and, when applicable, dosed with separate
723 freshly prepared dosing solutions. When applicable, dosing groups for each experimental replicate were
724 composed of siblings, such that sibling controls could be compared to dosed siblings. Statistical analyses
725 for each figure are listed in the accompanying figure legends. When comparing two groups, unpaired t-tests
726 with Welch's correction were performed, which is used when two samples have unequal variance and
727 sample size and therefore does not assume equal standard deviations. When comparing three or more
728 groups, One-Way ANOVA was performed. All statistics were performed using GraphPad Prism (Dotmatics,
729 San Diego, CA).
730
731 **Data availability**
732 All data is available in the main text and supplementary materials. All targeted and untargeted metabolomics
733 files will be deposited into Metabolomics Workbench.
734

Acknowledgments

We thank Dr. William Talbot for sharing their *irf8*$^{st96/st96}$ mutant line with us. We also thank Rachel Cyr for excellent care and oversight of our zebrafish facility. Thank you to other members of the Plavicki lab for their discussions in input during various stages of this study. Lastly, thank you to the undergraduate trainees that were involved in the early coordination of this work, Rekha Dhillon-Richardson and Ratna Patel. This work was supported by a NIH K99/R00 (ES023848/ES2384), NIEHS Outstanding New Environmental Scientist (ONES) award, and cardiopulmonary vascular COBRE Phase II (2PG20GM103652) awarded to J.S.P. In addition, this work was supported by the Ruth L. Kirschstein Predoctoral Individual National Research Service Award (NRSA; F31HL156460) by the NHLBI awarded to S.E.P. S.E.P and N.R.M. were previously supported by the Brown University Environmental Pathology Training Grant (T32ES007272-26) from NIEHS. The Thermo LC-Orbitrap MS was partially funded by NSF Major Research Instrumentation (MRI) award CBET-1919870 to K.P. (PI) and J.S.P (Co-I).

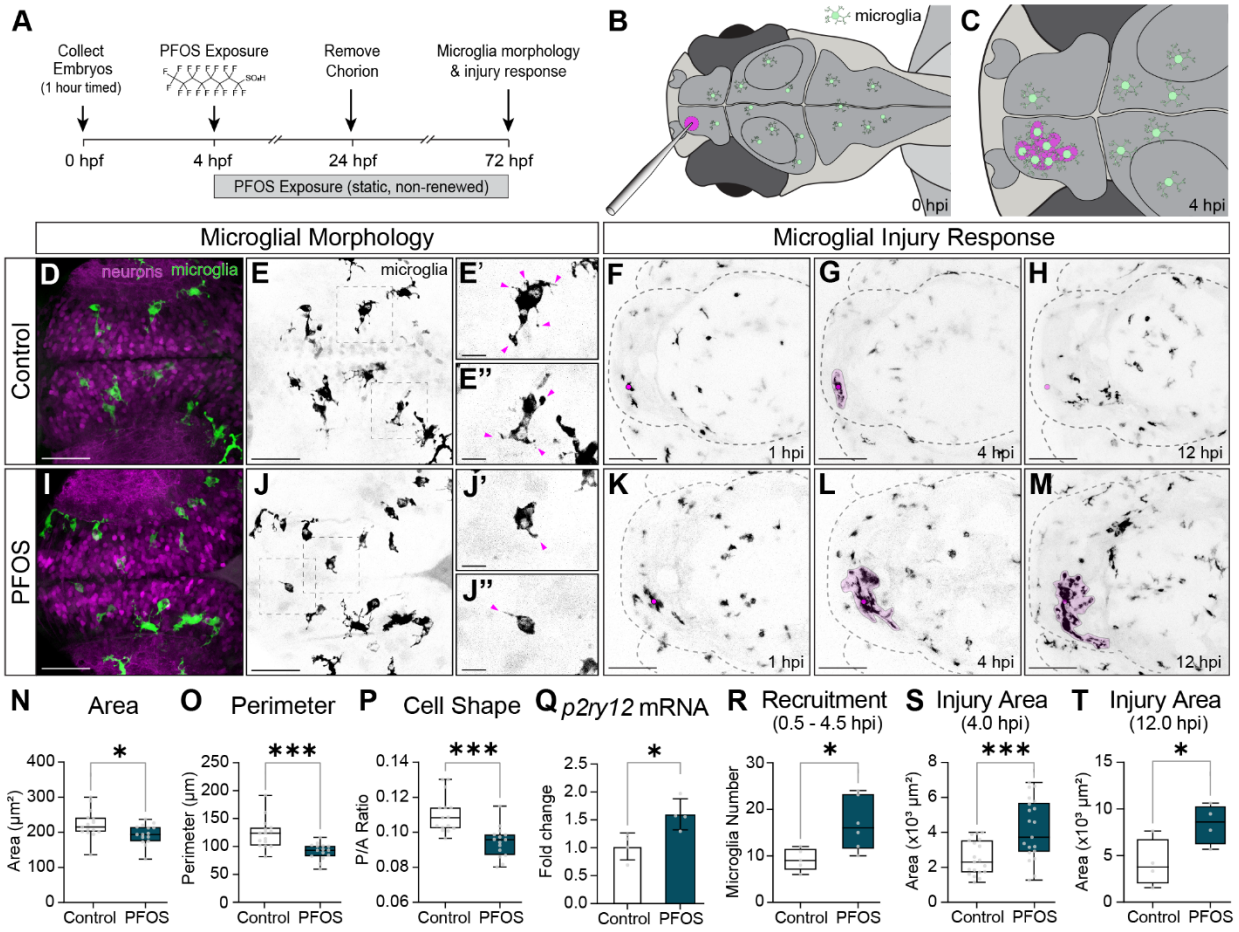

Figure 1. Microglia become activated and hyperresponsive to minor brain injury following developmental exposure to PFOS. (A) Exposure paradigm: zebrafish embryos from *Tg(mpeg1:EGFP)* adults were collected after a 1-hour timed spawn. At 4 hpf, embryos were dosed with 0.1% DMSO (Control) or 28 µM PFOS. Treatment solutions were static and not renewed. Embryos were dechorionated at 24 hpf, and imaging and injury experiments were conducted at 72 hpf. (B) Schematic of larval brain injury: a pulled glass needle (OD 9 um) was used to puncture the right telencephalon of larval zebrafish. (C) Hypothetical schematic of microglia response 4 hpi. (D-E") Homeostatic, non-activated microglia of 3 dpf control larvae have several projections emanating from their cell bodies. (F-H) Control microglia respond to brain injury, with visible accumulation at the injury site at 4 hpi that mostly clears by 12 hpi. (I-J") Microglia of 3 dpf larvae exposed to 28 µM PFOS become phenotypically activated, with rounder cell bodies and reduced projections. (K-M) In PFOS-exposed larvae, microglia robustly respond to brain injury by 4 hpi and are still maintained at the site at 12 hpi. Quantifications of the images reveal that PFOS-exposed microglia (N) area (P = 0.0342) and (O) cell perimeter (P = 0.0006) are significantly reduced. (P) The perimeter-to-area ratio (P = 0.0002) is also significantly decreased, indicative of a rounder cell morphology. n= 15 fish per group (3-18 cells counted per fish). (Q) qRT-PCR for the microglia activation gene, *p2ry12*, was significantly upregulated in isolated heads of PFOS-exposed larvae (P = 0.0205; n = 10 pooled heads per sample). PFOS exposure resulted in a significant increase in (R) microglia recruitment in the first 4.5 hpi (P = 0.0216; n = 5-6 per group), as well as increased response area at (S) 4 hpi (P = 0.0006; n = 19-20 per group) and (T) 12 hpi (P = 0.0467; n = 4 per group). Confocal micrographs at 40x magnification (D-E" & I-J") or 20x magnification (F-H; K-M). Unpaired t-test with Welch's correction.

785 Table 1. PFAS body burden in zebrafish larvae.

PFAS Body Burden (ng/embryo)

			Control		28 μM PFOS		56 μM PFOS	
Chemical	Formula	MW (g/mol)	48 hpf	72 hpf	48 hpf	72 hpf	48 hpf	72 hpf
PFOS	$C_8HF_{17}O_3S$	500.13	0.12 ± 0.17	0.12 ± 0.16	32.22 ± 2.57	**70.46 ± 2.72****	46.04 ± 3.75	**109.15 ± 5.99****
PFNS	$C_9HF_{19}O_3S$	550.14	0.01 ± 0.02	0.00 ± 0.00	0.19 ± 0.05	**0.39 ± 0.07****	0.23 ± 0.04	**0.69 ± 0.20*****
PFHpS	$C_7HF_{15}O_3S$	450.12	0.00 ± 0.00	0.00 ± 0.00	0.35 ± 0.17	0.45 ± 0.13	0.40 ± 0.17	**0.55 ± 0.11***
PFHxS	$C_6HF_{13}O_3S$	400.12	0.006 ± 0.012	0.008 ± 0.014	0.008 ± 0.014	0.007 ± 0.011	0.008 ± 0.012	0.008 ± 0.011

*p<0.05; ***p<0.001; ****p<0.0001

786

787
788
789
790
791
792
793

794 Table 2. Survival rate of zebrafish larvae exposed to 14 μM, 28 μM, or 56 μM PFOS over time.

795

Survival Rate Percentage

Age	PFOS Concentration			
	Control	14 μM	28 μM	56 μM
24 hpf	97.93 ± 2.94	97.67 ± 1.75	98.15 ± 1.73	97.22 ± 2.84
48 hpf	97.74 ± 2.76	97.14 ± 1.21	97.09 ± 2.10	92.49 ± 2.84
72 hpf	97.43 ± 3.25	96.18 ± 1.81	95.62 ± 2.43	81.54 ± 13.23
96 hpf	96.41 ± 5.82	95.72 ± 1.20	**50.65 ± 10.06***	**25.00 ± 9.89****
120 hpf	95.93 ± 5.85	89.14 ± 3.65	**7.73 ± 3.03*****	**5.33 ± 2.67*****

*p<0.05; **p<0.01; ****p<0.0001

796
797
798
799
800

801

802

803

804

805

806

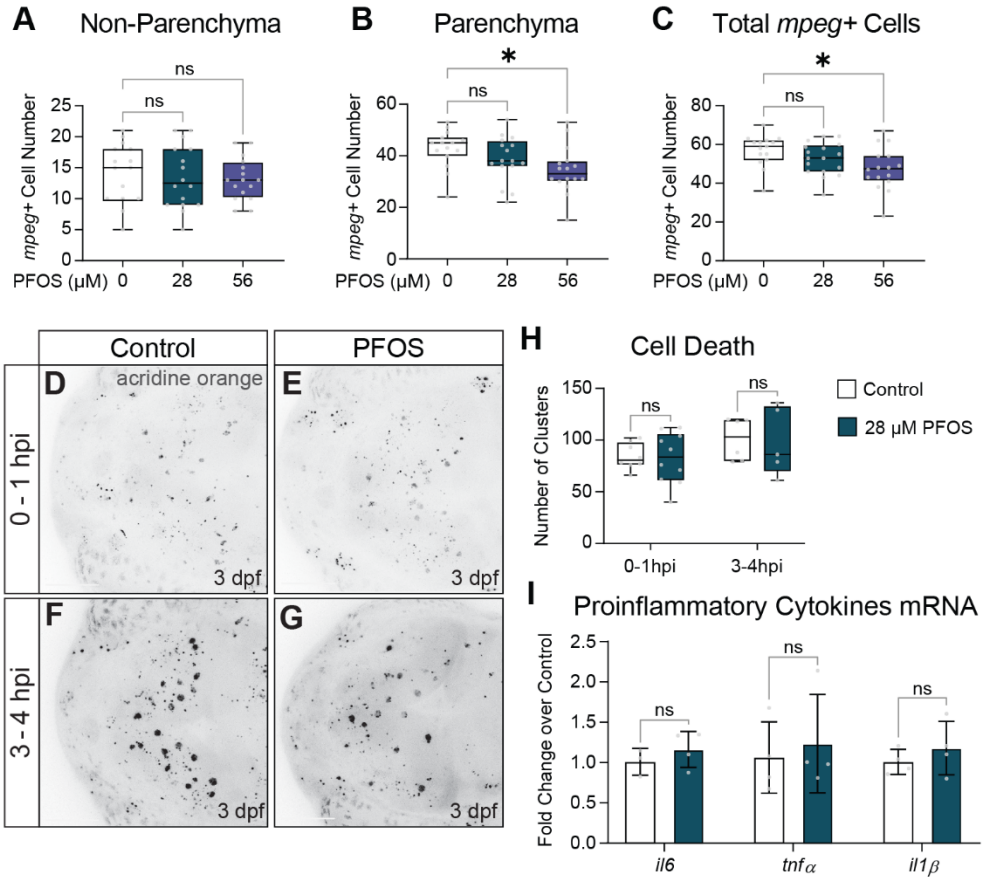

Figure 1-Supplement 1. Microglia hyperresponsiveness is not attributed to changes in microglia number, cell death, or brain inflammation. (A) Non-parenchymal, (B) parenchymal, and (C) total microglia on were quantified in 3 dpf control (n = 15), 28 μM PFOS (n = 16), or 56 μM PFOS (n = 16) exposed larvae. There was no significant difference in parenchymal or non-parenchymal microglia number in 28 μM PFOS-exposed larvae compared to controls, while 56 μM PFOS larvae had significantly fewer parenchymal (P = 0.0084) and total microglia (P = 0.0105). (D,E) To assess cell death, live 3 dpf larvae were stained with 5 ug/mL acridine orange during the first hour post injury or (F,G) between 3-4 hpi. (H) Quantification of acridine orange-positive clusters in 3 dpf control and 28 μM PFOS-exposed larvae show no significant change in cell death (n = 5-9 per group). (I) qRT-PCR for the inflammatory genes *il6*, *tnfα*, and *il1β* were not significantly changed in isolated heads of 3 dpf control or 28 μM PFOS-exposed larvae (n = 10 pooled heads per sample). Confocal micrographs at 20x magnification. Unpaired t-tests with Welch's correction. *P<0.05.

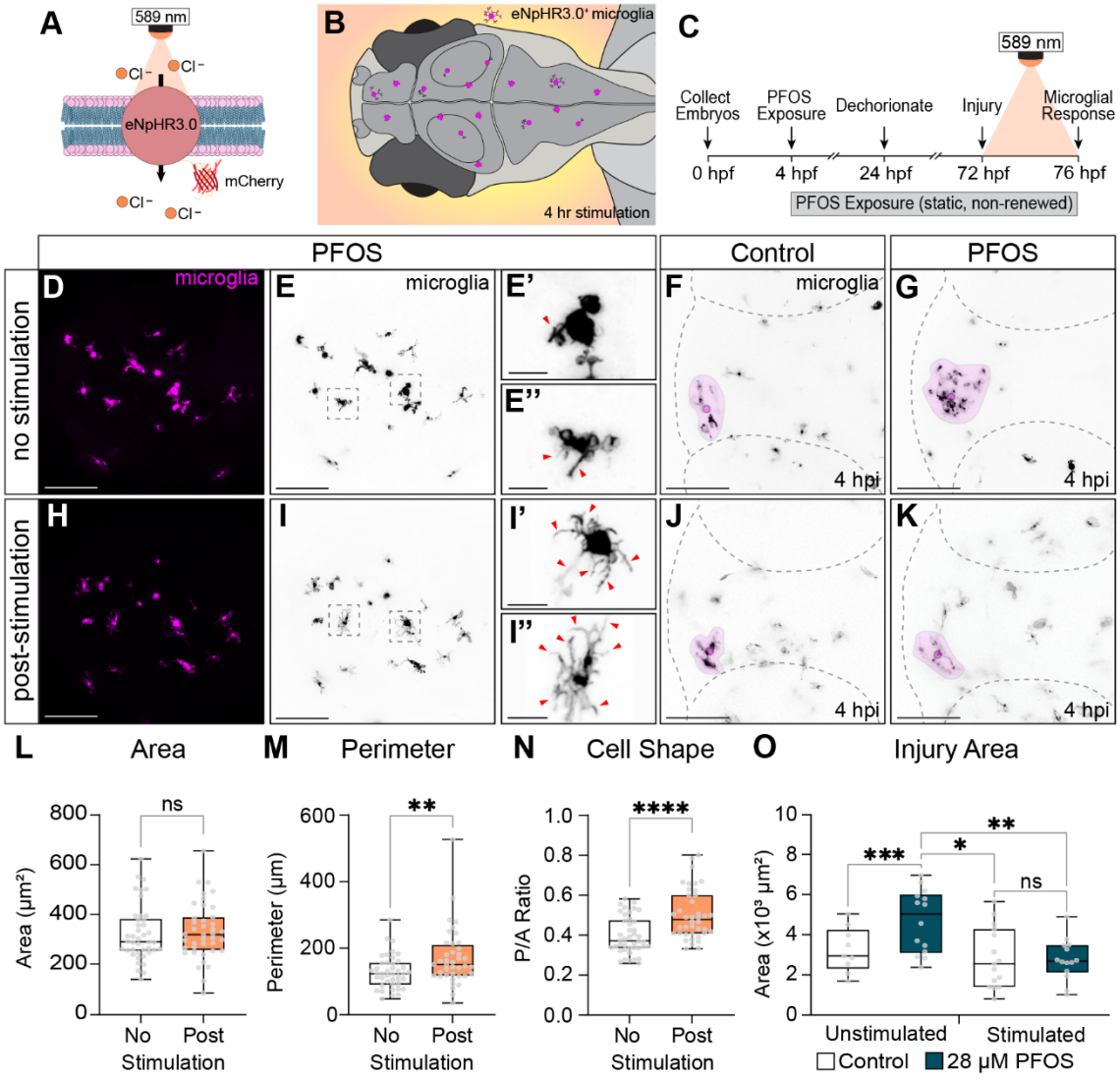

Figure 2. PFOS-induced microglia activation can be reverted by electrical modulation. (A) Schematic of halorhodopsin: Optogenetic modulation of microglia electrical state is achieved via photo-stimulation of the light-gated chloride pump, halorhodopsin (eNpHR3.0). eNpHR3.0 is most responsive to 589 nm wavelength light. (B) eNpHR3.0 was driven under a pan-macrophage promoter (*Tg(mpeg1:GalFF;UAS:eNpHR3.0-mCherry)*) to achieve optogenetic control of microglia in zebrafish larvae. (C) Experimental paradigm: At 72 hpf, injured or uninjured zebrafish were stimulated for 4 hours with 589 nm light in the enclosed Noldus DanioVision Behavior Unit. (D-E") Unstimulated halorhodopsin^{+} microglia of 3 dpf 28 μM PFOS-exposed larvae were rounded with few projections. As shown in Figure 1, (F) unstimulated control microglia were responsive to minor injury at 4 hpi, though (G) unstimulated PFOS-exposed microglia had a significantly heightened response. (H-I") Following 4-hour stimulation of halorhodopsin^{+} in PFOS-exposed larvae, microglia became more ramified. (J, K) Stimulation of halorhodopsin^{+} microglia following PFOS exposure also normalized the microglia response to injury. (L) Stimulated microglia area was unchanged, but (M) they had significantly increased cell perimeter (P = 0.0079) and (N) an increased perimeter-to-area ratio (P < 0.0001), indicative of a more ramified cell shape (n = 40-42 cells per group from 3 independent experiments). Unpaired t-tests with Welch's correction. (O) The injury response area was significantly increased between unstimulated control and 28 μM PFOS

841 exposed larvae (*P* = 0.0177); however, there was no significant difference in response area between 4-
842 hour stimulated control and PFOS-exposed larvae. Additionally, the stimulated PFOS-exposed area was
843 significantly decreased compared to the unstimulated PFOS group (*P* = 0.0008; n = 9-15 per group). One-
844 way ANOVA.

845

846

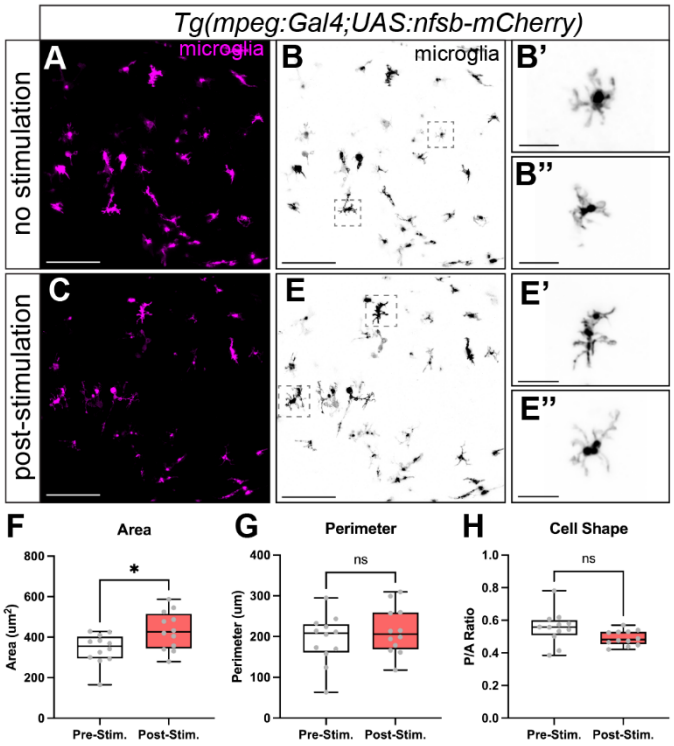

847

848 **Figure 2-Supplement 1. Light stimulation alone does not impact microglia morphology.** To ensure
849 that 589 nm light alone does not alter microglia morphology, PFOS-exposed transgenic larvae expressing
850 macrophage-driven mCherry (*Tg(mpeg1:gal4FF;UAS:nfsb-mCherry)*) were either (A-B'') unstimulated or
851 (C-E'') subjected to the 589 nm light for 4 hours. (F) While microglia area was increased following light
852 exposure (**P* < 0.05), (G) the light stimulation did not result in significant changes in perimeter or (H) the
853 perimeter-to-area ratio. Therefore, light stimulation alone does not result in the ramification of microglia. n
854 = 12 cells. Unpaired t-test with Welch's correction.

855

856

857

858

859

860

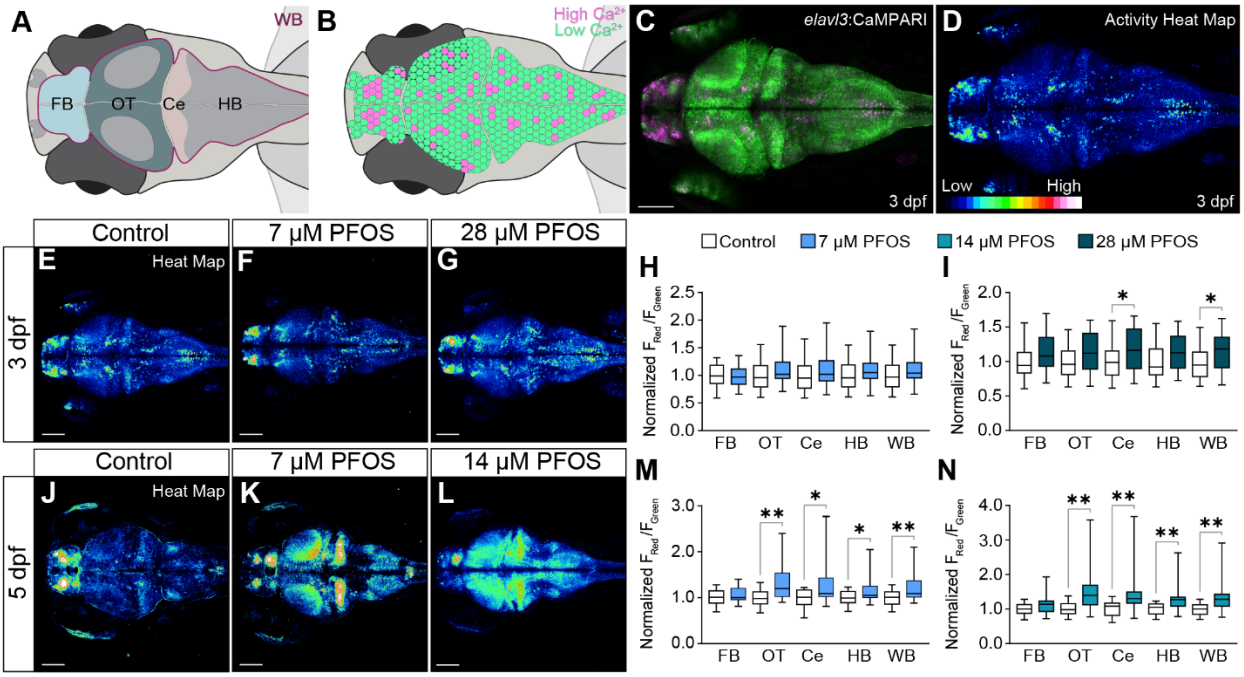

Figure 3. Developmental PFOS exposure alters global and regional neuronal network activity. (A) Illustrative representation of a larval zebrafish brain with anatomical regions outlined: forebrain (FB), optic tectum (OT), cerebellum (Ce), hindbrain (HB), and whole brain (WB). (B) Illustrative representation of neuron-driven CaMPARI: neurons with low intracellular calcium (low Ca^{2+}) remain green following 1 minute exposure to 405 nm light, while neurons with high intracellular calcium (high Ca^{2+}) are photoconverted to red. (C) Confocal micrograph of a 3 dpf larvae expressing neuron-specific CaMPARI (*Tg(elavl1:CaMPARI)*) following 1 minute photoconversion. (D) Generated high intensity LUTs heat map of the red, photoconverted channel in C depicting high activity neurons. Low to high Intracellular calcium is depicted by a blue-red-white spectrum. (E) Micrographs of active neurons at 3 dpf in control, (F) 7 µM PFOS, and (G) 28 µM PFOS larvae following 1-minute photoconversion. Neuronal activity can be quantified by determining the ratio of fluorescent intensity in the red versus green channels (F_{Red}/F_{Green}). (H) 7 µM PFOS does not result in a regional or global (WB) change in neuron activity in 3 dpf larvae. However, (I) 28 µM PFOS-exposed 3 dpf larvae demonstrate a modest increase in regional brain activity, and a significant increase in the Ce (P = 0.0483) and globally (WB; P = 0.0429). (J) Brain activity was also determined in 5 dpf larvae exposed to control, (K) 7 µM PFOS, or (L) 14 µM PFOS. At 5 dpf (M) 7 µM PFOS-exposed larvae have significant increases in brain activity in the OT (P = 0.0016), Ce (P = 0.0221), HB (P = 0.0294), and globally (P = 0.0075). (N) Larvae exposed to 14 µM PFOS also had increases in the OT (P = 0.0025), Ce (P = 0.0050), HB (P = 0.0038), and globally (P = 0.0036). Confocal micrographs at 10x magnification. n = 21-23 fish per group. Unpaired t-test with Welch's correction.

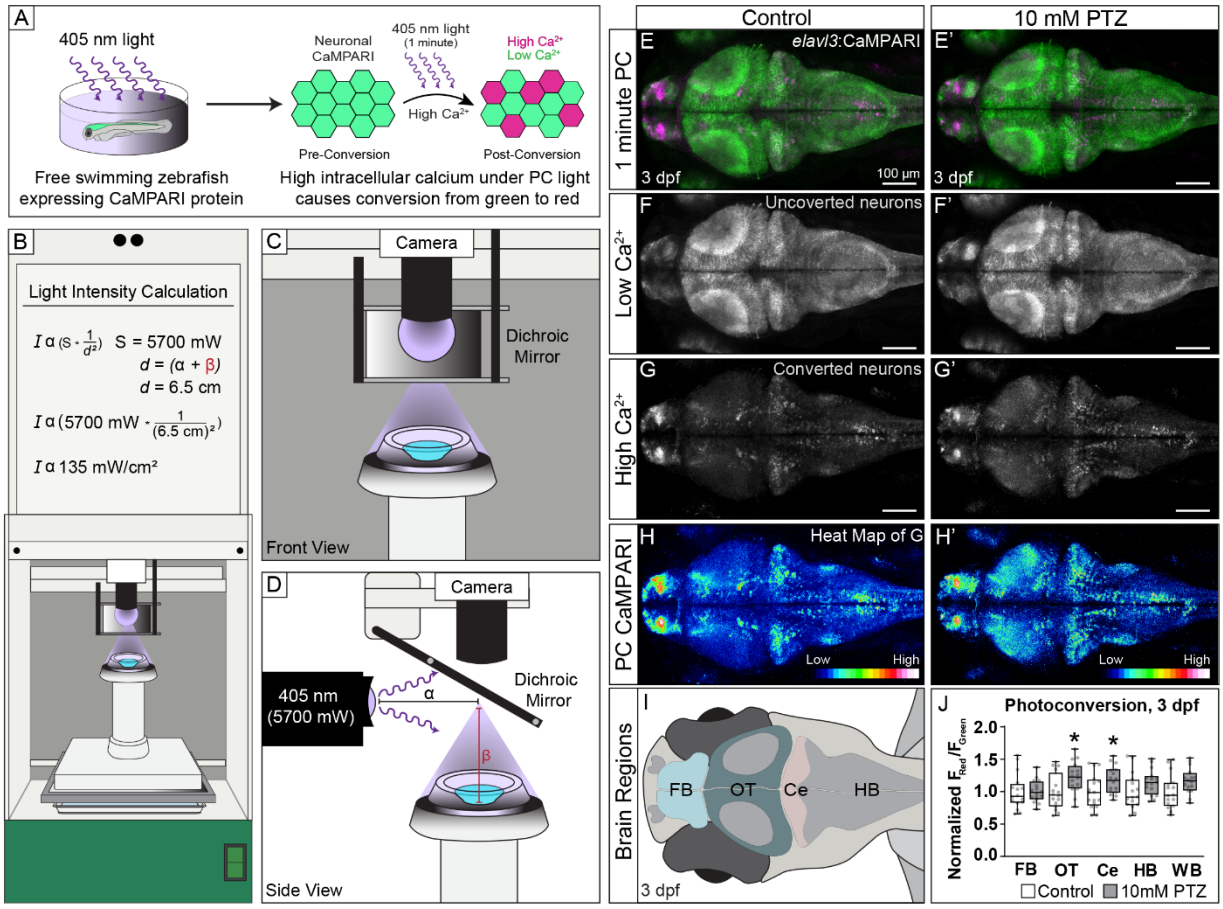

Figure 3- Supplement 1. Functional neuroimaging to understand the effects of toxicant exposure on neuronal activity. (A) Schematic overview of CaMPARI photoconversion: free-swimming zebrafish larvae with neuron-specific expression of the genetically encoded calcium indicator CaMPARI protein (*Tg(elavl3:CaMPARI)*) are subjected to 405 nm light for 1 minute. Exposure to blue light photoconverts any neurons with high intracellular calcium from green to red. (B-D) We modified our Noldus DanioVision Behavioral unit, outfitted with LEDs for optogenetic manipulation, to efficiently photoconvert CaMPARI in free-swimming zebrafish. (B) A 3D printed pedestal is used to reduce the working distance between the light source and zebrafish larvae. Applying the inverse-square law, the light intensity at the apex of the pedestal was calculated to be 135 mW/cm². (C) Illustration of the apex of the pedestal containing a single well dish (OD 15 mm). (D) The 405 nm light has an intensity of 5700 mW at the source. The light travels horizontally then is reflected off a dichroic mirror within the unit. The working distance was calculated as the distance from the light source to the dichroic mirror (α) plus the distance from the dichroic mirror to the apex of the pedestal (β). (E) Confocal micrographs of neuronal calcium following 1-minute photoconversion of CaMPARI in 3 dpf larvae treated with egg water or (E') after 10 minutes in 10 mM pentylenetetrazol (PTZ), a GABAA-inhibitor known to induce hyperactivity. (F, F') Green, non-active neurons with low intracellular calcium from E & E'. (G, G') Photoconverted, active neurons with high intracellular calcium, pseudo-labeled as magenta, from E & E'. (H, H') An intensity LUTs applied to the active neurons in G & G' spectrally maps the regional increases of neuronal activity on a scale from less active (blue) to more active (red-white). (I&J) Regional and global neuronal activity can be quantified by determining the ratio of fluorescent intensity in the red versus green channel (F_{Red}/F_{Green}). Exposure to 10 mM PTZ significantly increased brain activity in the optic tectum (OT; $P = 0.0200$), cerebellum (Ce; $P = 0.0386$), and nearly in the

whole brain (WB; *P* = 0.0501), but not in the forebrain (FB) or hindbrain (HB). Red/Green ratios were normalized relative to vehicle control. n =16 fish per group. Unpaired t-test with Welch's correction.

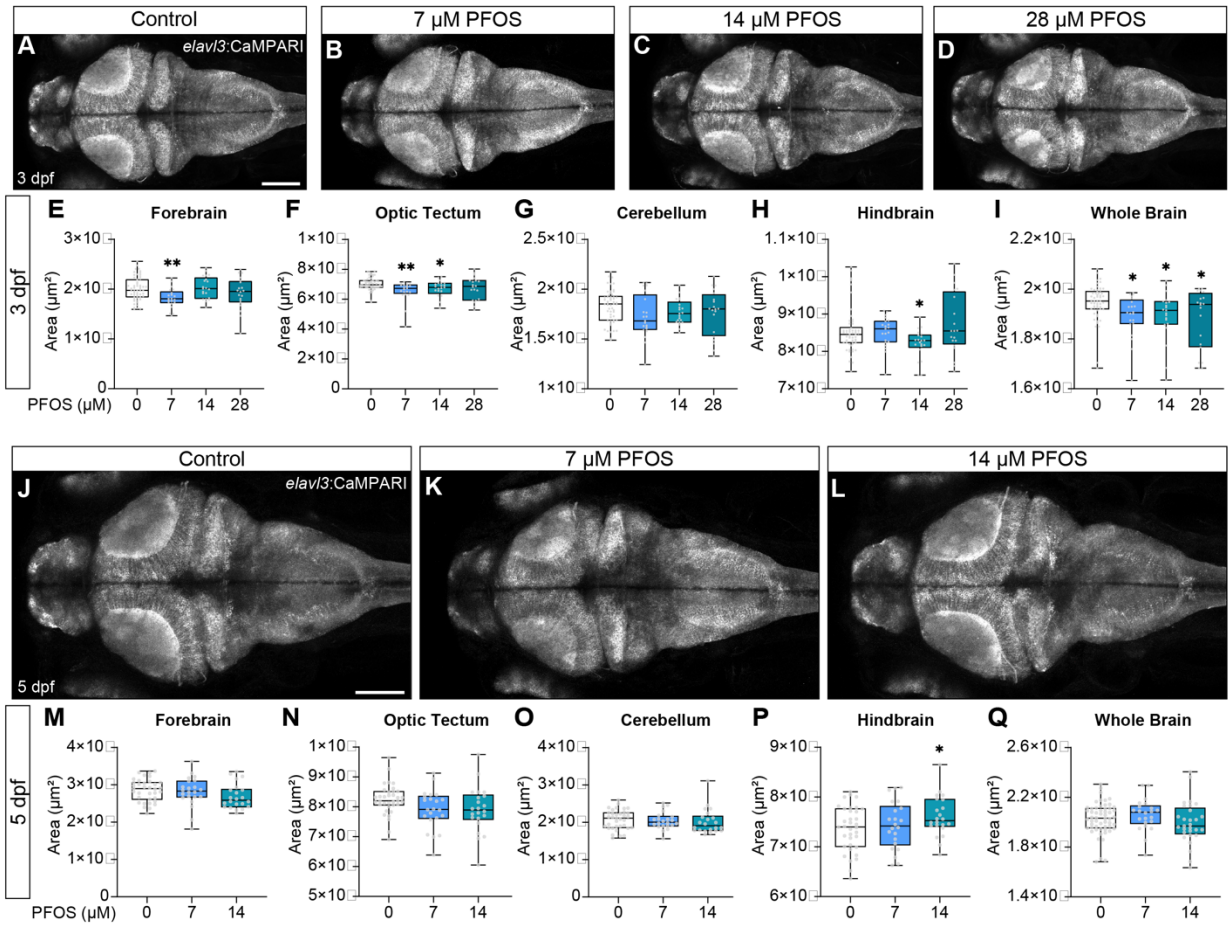

Figure 3-Supplement 2. PFOS exposure does not significantly affect larval brain morphology over time. (A-D) Confocal micrographs of 3 dpf larvae or (J-L) 5 dpf larvae expressing *Tg(elavl3:CaMPARI)* exposed to (A&J) control, (B&K) 7 µM, (C&L) 14 µM, or (D) 28 µM PFOS. At 3 dpf, 7 µM PFOS larvae had a significant reduction in area of the (E) forebrain (Control vs 7 µM PFOS, *P* = 0.0012) and (F) optic tectum (Control vs 7 µM PFOS, *P* = 0.0052). Additionally, 3 dpf 14uM PFOS-exposed larvae had significant reduction in areas of the (F) optic tectum (Control vs 14 µM PFOS, *P* = 0.015) and (H) hindbrain (Control vs 14 µM PFOS, *P* = 0.019). (I) When measuring the area of the entire brain, all three concentrations of PFOS resulted in reduced global brain area (Control vs 7 µM, 14 µM, 28 µM, *P* = 0.013; *P* = 0.030; *P* = 0.030, respectively). (P) At 5 dpf, the only significantly affected regional area was the hindbrain following exposure to 14 µM PFOS (Control vs 14 µM PFOS, *P* = 0.036). (Q) There was no significant change in global brain area at 5 dpf with 7 µM nor 14 µM PFOS exposure. Confocal micrographs at 10x magnification. Control n = 52-54; treated n = 22-25. Statistical analysis determined by Welch One-Way ANOVA. *P<0.05; **P<0.01. Scale bar = 100 um.

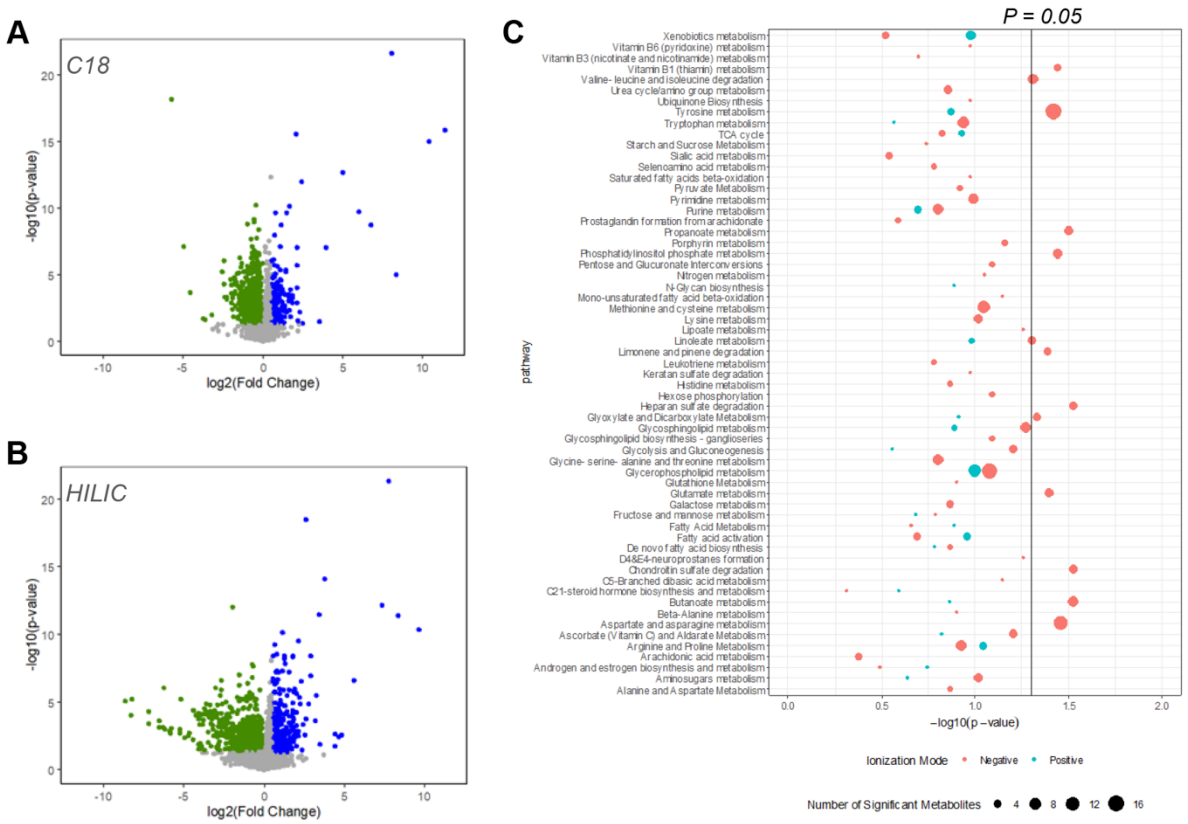

Figure 3-Supplement 3. MWAS of heads collected from control versus PFOS-exposed larvae. Heads were collected from 3 dpf control or 28 μM PFOS exposed larvae for an untargeted metabolome wide association study (MWAS). (A) Volcano plots of metabolites detected using a C18 column with negative ionization and (B) a HILIC column with positive ionization reveal several significantly down- or up-regulated metabolites in the PFOS-exposed brain (Green = downregulated; Blue = upregulated). Statistical significance was set at $P = 0.05$. (C) There are several significantly enriched pathways following both negative ionization (pink) and positive ionization (teal). The vertical line is at $P = 0.05$. Size of each dot represents the number of significant metabolites in that pathway. HILIC, hydrophilic interaction liquid chromatography column.

952 Table 3. Significantly enriched metabolic pathways following PFOS exposure in 3 dpf larvae
953
954

Significantly Enriched Pathway	Physiological Relevance in CNS	Source
Vitamin B1 (thiamin) metabolism	- Microglia regulation - Neuronal K^+ channels regulation - Myelinogenesis - Improves cognitive function	(Ba 2008, Mkrtchyan et al. 2015)
Valine-leucine and isoleucine degradation	- Neurotransmitter metabolism, including glutamate - Protein synthesis and energy production - Nitrogen homeostasis and neurotransmitter cycling	(Polis and Samson 2020, Salcedo et al. 2021)
Tyrosine metabolism	- Catecholamine synthesis - Regulator of neuronal longevity	(Kobayashi et al. 1995) (Parkhitko et al. 2020)
Propanoate metabolism	- Modulates glutamine synthetase in glia - Inhibits histone deacetylase in GABAergic neurons, increasing GABA levels	(Morland et al. 2018, Nguyen et al. 2007)
Phosphatidylinositol phosphate metabolism	- Neurotransmitter receptor expression regulation - Synaptic vesicle regulation and recycling - Neurite and dendrite morphogenesis - Clathrin-dependent membrane trafficking - Ion channel and transporter activity regulation	(Clayton, Minogue and Waugh 2013, Raghu et al. 2019)
Linoleate metabolism	- Modulates astrocyte inflammatory response - Stimulates axonal growth of cortical neurons	(Saba et al. 2019, Hennebelle et al. 2020)
Limonene and pinene degradation	- Represses neuronal cell death - Decreases activated glial cell number - Involved in neuroprotection - Anti-inflammatory and analgesic roles	(Eddin et al. 2021)
Heparan sulfate degradation	- Regulator of axon guidance and synapse development and specificity - Involved in regulating the dopamine system - Part of the core synaptic organizing complexes neurexin and neuroligin	(Condomitti and de Wit 2018, De Risi et al. 2021)
Glyoxylate and dicarboxylate metabolism	- Important for carbohydrate metabolism and energy availability - Altered following traumatic brain injury	(Baker et al. 2018)

Glutamate metabolism	- Involved in nitrogen trafficking and ammonia homeostasis in brain - Excitatory neurotransmitter and immediate precursor for the neurotransmitter GABA	(Schousboe et al. 2014)
Chondroitin sulfate degradation	- Role in development, plasticity, and regulation of cortical circuitry - Modulates ion channel properties - Inhibits structural plasticity (scar after injury, axonal pathfinding, and synapse formation during development) - Neuronal excitability modulation	(Hudson et al. 2015)
Butanoate metabolism	- Neuromodulator largely produced by gut microbiota - Attenuates neuronal apoptosis - Inhibits amyloidogenesis - Protects neurons from ischemic damage - Improves long-term memory - Neurodegenerative attenuation	(Kim et al. 2020, Xu et al. 2021, Zhou et al. 2021)
Aspartate and asparagine metabolism	- Secondary excitatory neurotransmission - Amino acid involved in glutamate synthesis - Influences NMDAR-mediated transmission - Can evoke presynaptic release of endogenous l-glutamate release in selective brain regions - Synaptic strength and connectivity modulation	(Pardo et al. 2011, Errico et al. 2018)

955
956

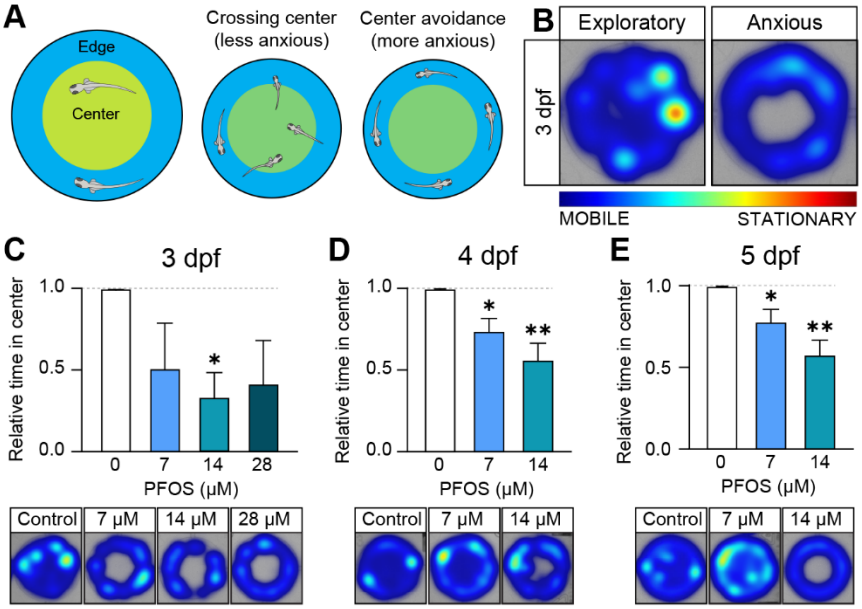

Figure 4. Developmental PFOS exposure increases anxiety-like behaviors. (A) Larval swim behavior during a 30-minute photomotor response assay can be interrogated to determine time spent in the well's center (crossing center; less anxious) versus time spent along the well's edge (center avoidance; more anxious). (B) Heat maps were generated to indicate mobile (blue) versus stationary (red) swim activity within the well, as well as the areas traversed within the well. (C) At 3 dpf, larvae exposed to 7 μM and 28 μM PFOS spend considerably less time in the center of the wells, and 14 μM PFOS spend significantly less time in the center ($P = 0.0232$). (D) At 4 dpf, both 7 μM ($P = 0.0410$) and 14 μM ($P = 0.0018$) PFOS-exposed larvae spend significantly less time in the center compared to control larvae. (E) This is also true in 5 dpf larvae exposed to 7 μM ($P = 0.0440$) and 14 μM PFOS ($P = 0.0013$). n = 76-101 fish per group. Unpaired t-test with Welch's correction. Error bars represent SEM.

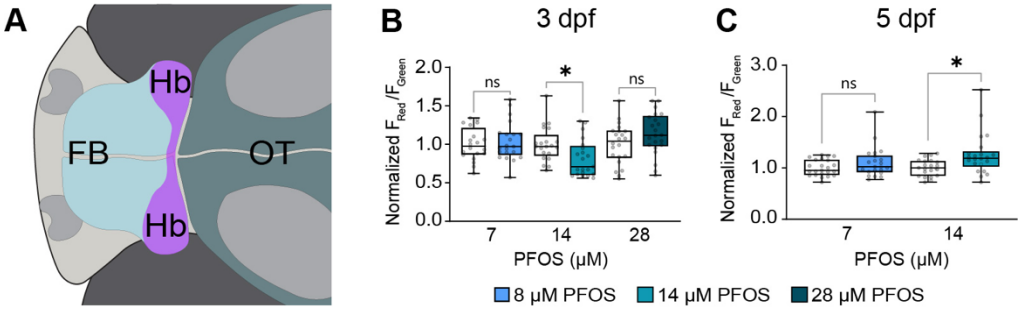

Figure 4- Supplement 2. (A) Illustrative representation of a larval zebrafish brain with anatomical regions outlined: forebrain (FB), habenula (Hb), and the optic tectum (OT). Activity quantification of neuron-driven CaMPARI was performed in the entire developing habenula following 1-minute exposure to 405 nm light. (B) At 3 dpf, 14 μM PFOS exposure caused a significant decrease in habenular Ca^{2+} activity ($P = 0.0138$), but not 7 μM nor 28 μM PFOS. (C) At 5 dpf, 14 μM PFOS-exposed larvae had a significant increase in habenular Ca^{2+} activity ($P = 0.0101$), but not 7 μM PFOS. n = 20-22 fish per treatment. Unpaired t-test with Welch's correction.

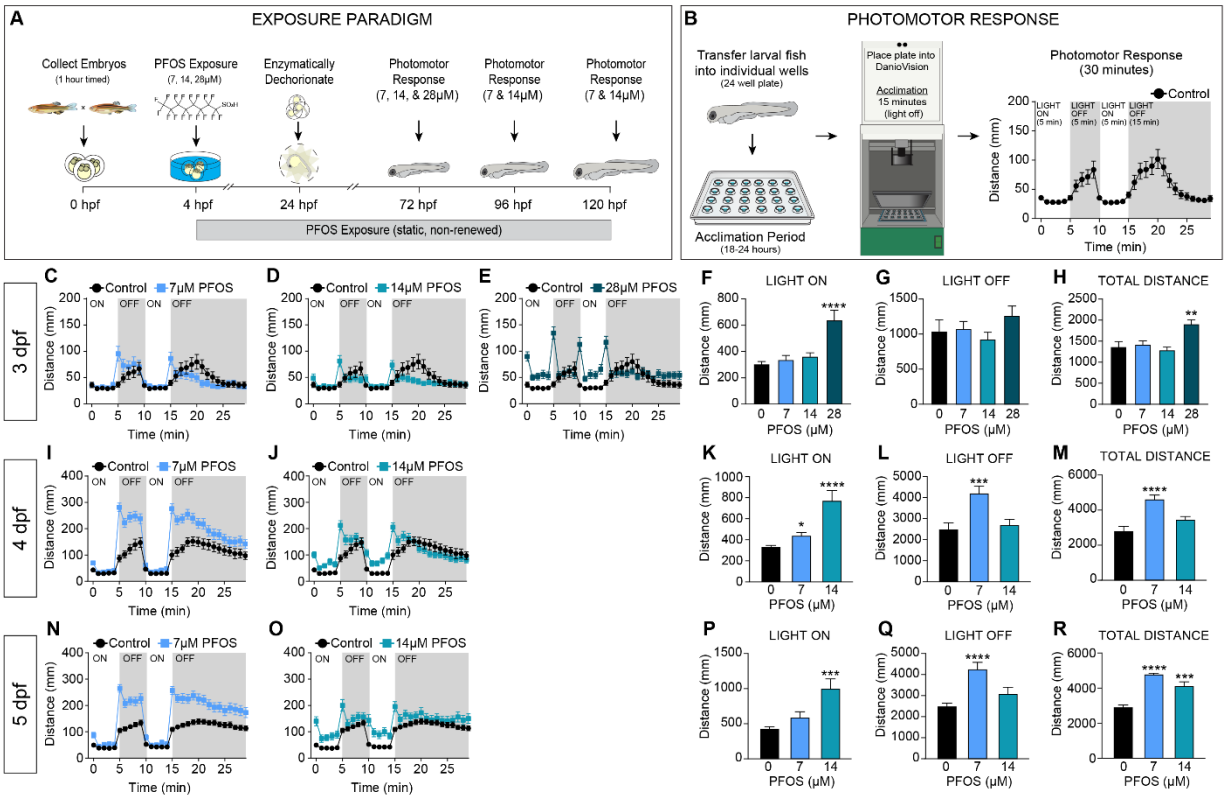

Figure 4-Supplement 1. Developmental PFOS exposure increases larval zebrafish behavior. (A) Exposure paradigm: at 4 hpf, zebrafish embryos were statically exposed to 0.1% DMSO (Control) or varying concentrations of PFOS (7, 14, or 28 μM). At 24 hpf, embryos were enzymatically dechorionated. Behavior was captured at 72, 96, and 120 hpf. (B) Photomotor response assay: Zebrafish larvae were placed in individual wells of a 24-well plate 18-24 hours prior to the behavior assay to allow for well acclimation. A photomotor assay was performed using the Noldus DanioVision Behavioral Unit. The photomotor assay was as follows: 15-minute acclimation in the unit with the light off, 5 minutes with the light on, 5 minutes with the light off, 5 minutes with the light on, and 15 minutes with the light off. (C-H) At 3 dpf, larvae exposed to 28 μM PFOS had a significant increase in swim activity during the (F) light on cycles ($P < 0.0001$) and (H) over the course of the assay ($P = 0.0023$). (K) At 4 dpf, 7 μM PFOS larvae had a significant increase in swim distance when the light was on ($P = 0.0103$), as did 14 μM PFOS larvae ($P < 0.0001$). (L) At 4 dpf, 7 μM PFOS-exposed larvae also had a significant increase in swim behavior when the light was off ($P = 0.0006$) and (M) in total over the course of the assay ($P < 0.0001$). (P) At 5dpf, 14 μM PFOS had increased swim behavior when the light was on ($P = 0.0002$), and (Q) 7 μM PFOS larvae had increased swim behavior when the light was off ($P < 0.0001$). (R) Both 7 μM ($P < 0.0001$) and 14 μM PFOS ($P = 0.0001$) larvae had a significant increase in total distance moved. n = 130-190 for controls, n = 88-99 for PFOS-expose. One-way ANOVA. Multiple comparisons were performed using Tukey's multiple comparisons test.

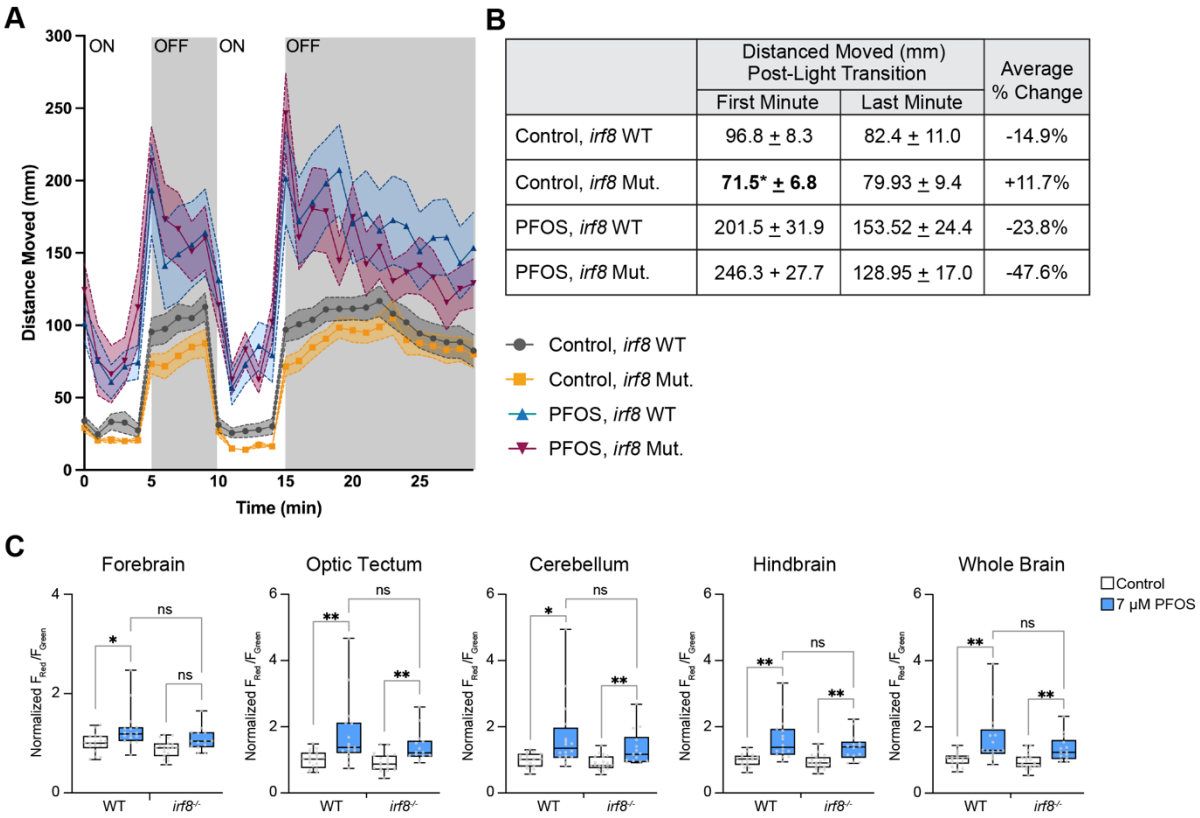

	Distanced Moved (mm) Post-Light Transition		Average % Change
	First Minute	Last Minute	
Control, *irf8* WT	96.8 ± 8.3	82.4 ± 11.0	-14.9%
Control, *irf8* Mut.	**71.5* ± 6.8**	79.93 ± 9.4	+11.7%
PFOS, *irf8* WT	201.5 ± 31.9	153.52 ± 24.4	-23.8%
PFOS, *irf8* Mut.	246.3 + 27.7	128.95 ± 17.0	-47.6%

Figure 5. Microglia may influence larval behavior but are not responsible for PFOS-induced behavioral or neuronal phenotypes. Wildtype and microglia-deficient *irf8*$^{st96/st96}$ larvae dosed with either control or 7 µM PFOS were assessed for potential changes in swim behavior and neuronal activity. (A) Photomotor response assay of 5 dpf wildtype or *irf8* mutant control or PFOS-exposed larvae. (B) Assessing the distance moved following the first minute of the second light "off" cycle (i.e., minute 15 of the assay), control-treated *irf8* mutant larvae responded significantly less than wildtype controls (P = 0.0237). While not significant, PFOS-exposed *irf8* mutants had a heightened response to the first minute of the dark cycle compared to PFOS-exposed wildtype larvae. PFOS mutants also had twice the percent recovery in swim activity by the last minute of the assay (i.e., minute 15 versus minute 30). (C) There were no significant differences in regional or global PFOS-induced neuronal hyperactivity between the wildtype or mutant larvae expressing *Tg*(*elavl3:CaMPARI*). Unpaired t-test with Welch's correction. n = 14-22 per group for behavior; n = 13-16 per group for neuroimaging.

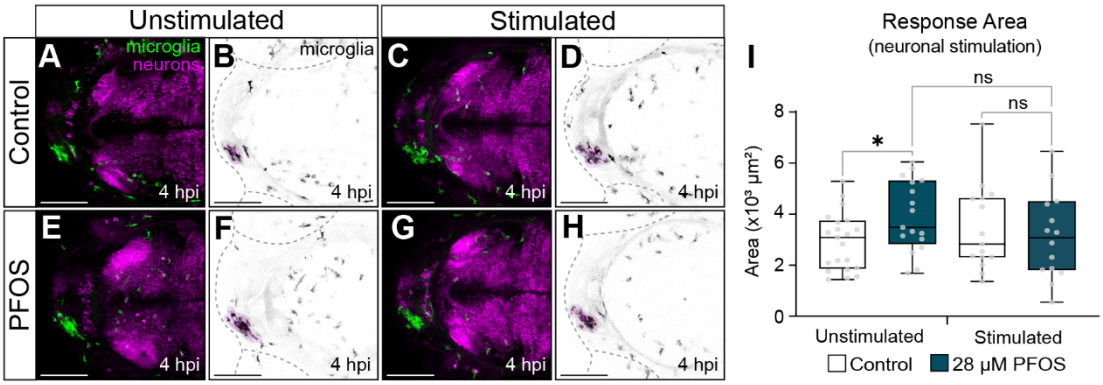

Figure 6. Neuronal silencing normalizes microglia responsiveness in PFOS-exposed larvae. Larvae expressing *Tg(elavl3:Gal4;cryaa:RFP;UAS:eNpHR3.0;mpeg1:EGFP)* were dosed with (A-D) control or (E-H) 28 µM PFOS and injured at the right telencephalon at 3 dpf and imaged 4 hpi. (E&F) PFOS-exposed unstimulated larvae had a significant increase in microglia response compared to controls (P = 0.0256). (C&D) Optogenetic stimulation of halorhodopsin with 570 nm light for 4 hpi did not affect microglia response to injury in control larvae. (G&H) However, neuronal silencing in PFOS-exposed larvae normalized the microglia response, such that the response was equivalent to the stimulated controls. (I) Quantification of microglia response area. Unpaired t-test with Welch's correction. n = 14-20 per group.

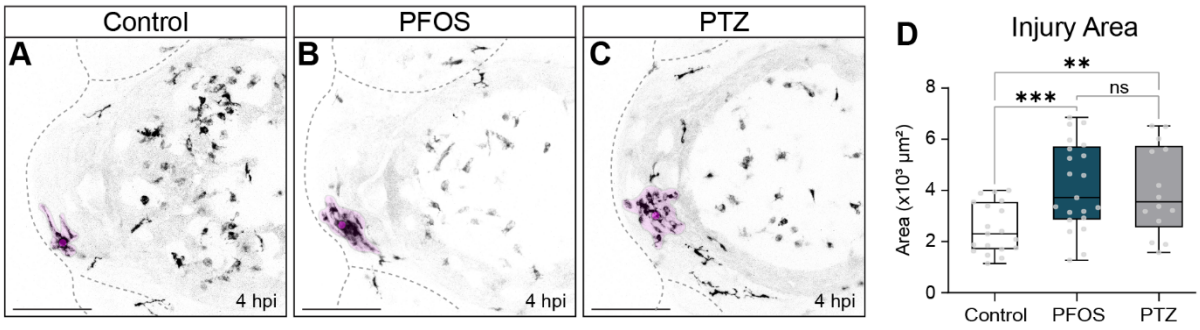

Figure 6-Supplement 1. Neuronal excitation recapitulates microglia hyperresponsive phenotype seen in PFOS-exposure. Larvae with transgenic expression of macrophages (Tg(*mpeg1:EGFP*)) were dosed with either (A) control or (B) 28 µM PFOS at 4 hpf, or (C) 5 mM PTZ at 72 hpf, followed by brain injury. (D) At 4 hpi, PFOS-exposed larvae had a significant increase in microglia response area (P = 0.0006). In addition, neuronal excitation by PTZ also resulted in a significant increase in microglia response (P = 0.0092). Unpaired t-test with Welch's correction. n = 14-21 per group.

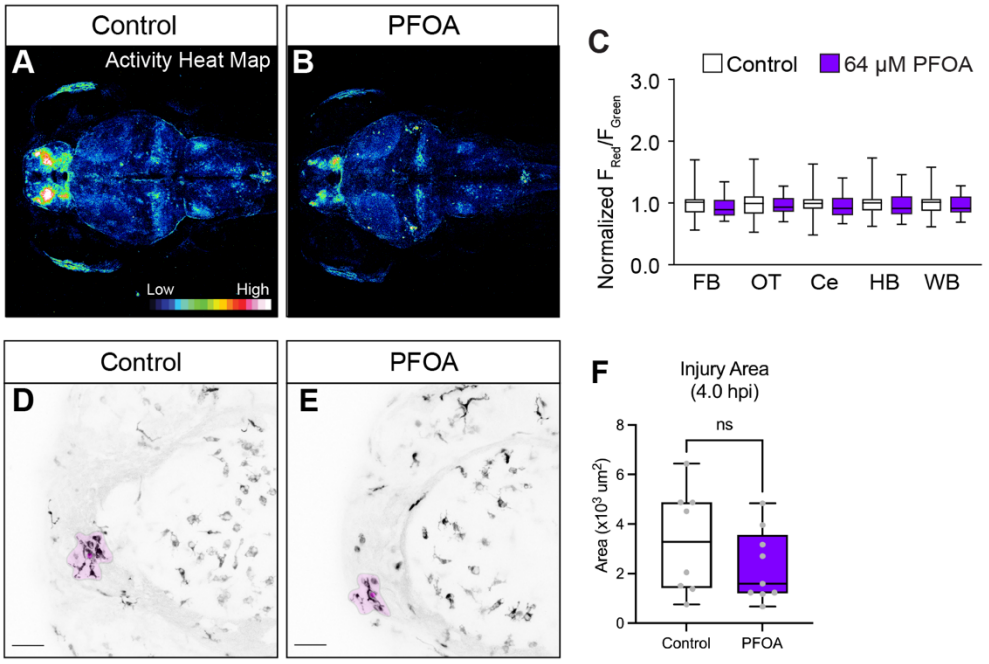

Figure 7. Exposure to a non-excitatory PFAS does not result in microglia hyperresponsiveness. PFOA is an 8-carbon PFAS compound with a carboxylate head group. To observe the effects of PFOA on neuronal activity, we again used larvae of the Tg(*elavl3:CaMPARI*) background. (A) At 5 dpf, control and (B) 64 µM PFOA-exposed larvae show no significant changes in regional or global neuronal activity, quantified in (C). (D) Larvae expressing Tg*(mpeg1:EGFP)* were also dosed with control solution or (E) 64 µM PFOA to determine if this non-excitatory PFAS compound resulted in microglia response differences. (F) At 4hpi, 64 µM PFOA-exposed larvae did not have a significant change in microglia response to injury compared to sibling controls. n = 8-9 per group. Unpaired t-test with Welch's correction.

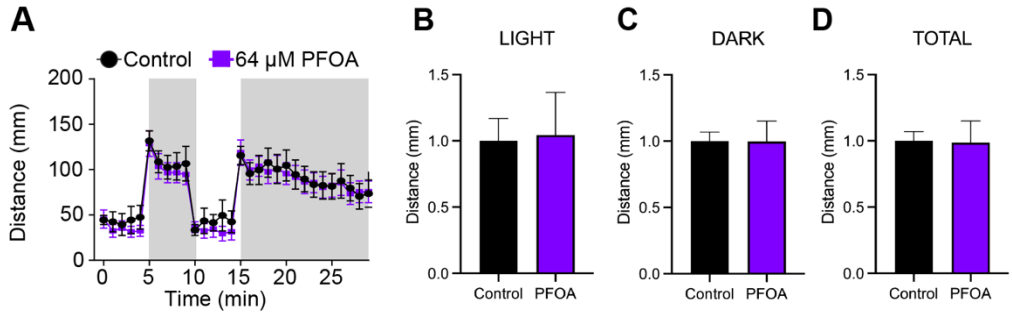

Figure 7-Supplement 1. PFOA exposure does not increase zebrafish swim behavior. Zebrafish larvae were subjected to a 30-minute photomotor response assay at 5 dpf, as previously described. (A) There were no apparent changes in distance moved during the 30-minute assay. (B) Total distance moved during light cycles, (C) dark cycles, and (D) in total throughout the assay were not significantly changed. n = 24 for controls, n = 46 for PFOA exposed. Unpaired t-test with Welch's correction.

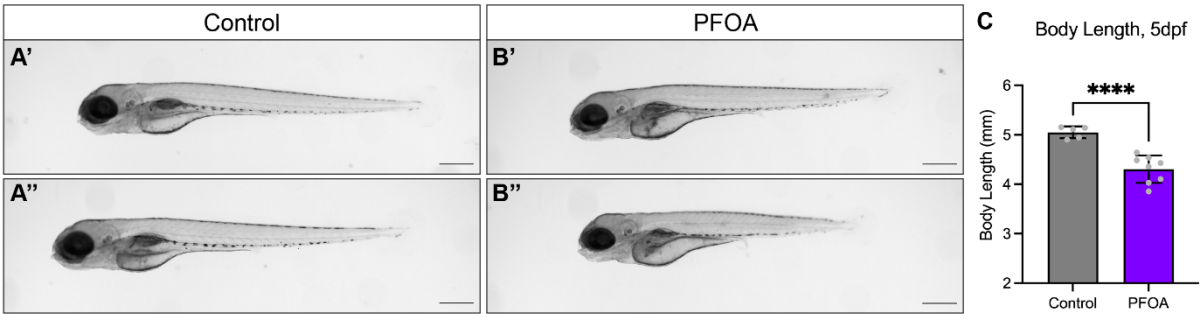

Figure 7-Supplement 2. PFOA exposure does not result in morphological changes that would impact swim ability. (A'-A'') Images of 5 dpf control-treated larvae. (B'-B'') Images of 5 dpf larvae chronically treated with 64 µM PFOA. (C) Body length measurements of control versus PFOA treatment at 5 dpf ($P < 0.0001$). Unpaired t-test with Welch's correction. n = 5-8 per group. Scale = 500 um.

References

Ahmad, F. & M. K. Richardson (2013) Exploratory behaviour in the open field test adapted for larval zebrafish: impact of environmental complexity. *Behav Processes,* 92**,** 88-98.

Antinucci, P., A. Dumitrescu, C. Deleuze, H. J. Morley, K. Leung, T. Hagley, F. Kubo, H. Baier, I. H. Bianco & C. Wyart (2020) A calibrated optogenetic toolbox of stable zebrafish opsin lines. *Elife,* 9.

Armada-Moreira, A., J. I. Gomes, C. C. Pina, O. K. Savchak, J. Goncalves-Ribeiro, N. Rei, S. Pinto, T. P. Morais, R. S. Martins, F. F. Ribeiro, A. M. Sebastiao, V. Crunelli & S. H. Vaz (2020) Going the Extra (Synaptic) Mile: Excitotoxicity as the Road Toward Neurodegenerative Diseases. *Front Cell Neurosci,* 14**,** 90.

Arrenberg, A. B., F. Del Bene & H. Baier (2009) Optical control of zebrafish behavior with halorhodopsin. *Proc Natl Acad Sci U S A,* 106**,** 17968-73.

Ba, A. (2008) Metabolic and structural role of thiamine in nervous tissues. *Cell Mol Neurobiol,* 28**,** 923-31.

Badimon, A., H. J. Strasburger, P. Ayata, X. Chen, A. Nair, A. Ikegami, P. Hwang, A. T. Chan, S. M. Graves, J. O. Uweru, C. Ledderose, M. G. Kutlu, M. A. Wheeler, A. Kahan, M. Ishikawa, Y. C. Wang, Y. E. Loh, J. X. Jiang, D. J. Surmeier, S. C. Robson, W. G. Junger, R. Sebra, E. S. Calipari, P. J. Kenny, U. B. Eyo, M. Colonna, F. J. Quintana, H. Wake, V. Gradinaru & A. Schaefer (2020) Negative feedback control of neuronal activity by microglia. *Nature,* 586**,** 417-423.

Baker, E. W., W. M. Henderson, H. A. Kinder, J. M. Hutcheson, S. R. Platt & F. D. West (2018) Scaled traumatic brain injury results in unique metabolomic signatures between gray matter, white matter, and serum in a piglet model. *PLoS One,* 13**,** e0206481.

Baraban, S. C., M. R. Taylor, P. A. Castro & H. Baier (2005) Pentylenetetrazole induced changes in zebrafish behavior, neural activity and c-fos expression. *Neuroscience,* 131**,** 759-68.

Braun, J. M. (2017) Early-life exposure to EDCs: role in childhood obesity and neurodevelopment. *Nat Rev Endocrinol,* 13**,** 161-173.

Browne, C. A., R. Hammack & I. Lucki (2018) Dysregulation of the Lateral Habenula in Major Depressive Disorder. *Front Synaptic Neurosci,* 10**,** 46.

Buck, R. C., J. Franklin, U. Berger, J. M. Conder, I. T. Cousins, P. de Voogt, A. A. Jensen, K. Kannan, S. A. Mabury & S. P. van Leeuwen (2011) Perfluoroalkyl and polyfluoroalkyl substances in the environment: terminology, classification, and origins. *Integr Environ Assess Manag,* 7**,** 513-41.

Bullard, R. D. (1994) Overcoming Racism in Environmental Decisionmaking. *Environment: Science and Policy for Sustainable Development,* 36**,** 10-44.

Castano-Ortiz, J. M., V. L. B. Jaspers & C. A. Waugh (2019) PFOS mediates immunomodulation in an avian cell line that can be mitigated via a virus infection. *BMC Vet Res,* 15**,** 214.

Chambers, W. S., J. G. Hopkins & S. M. Richards (2021) A Review of Per- and Polyfluorinated Alkyl Substance Impairment of Reproduction. *Front Toxicol,* 3**,** 732436.

Chang, E. T., H. O. Adami, P. Boffetta, H. J. Wedner & J. S. Mandel (2016) A critical review of perfluorooctanoate and perfluorooctanesulfonate exposure and immunological health conditions in humans. *Crit Rev Toxicol,* 46**,** 279-331.

Chen, J., R. L. Tanguay, T. L. Tal, Z. Gai, X. Ma, C. Bai, S. C. Tilton, D. Jin, D. Yang, C. Huang & Q. Dong (2014) Early life perfluorooctanesulphonic acid (PFOS) exposure impairs zebrafish organogenesis. *Aquat Toxicol,* 150**,** 124-32.

1118 Chong, J. & J. Xia (2018) MetaboAnalystR: an R package for flexible and reproducible analysis
1119 of metabolomics data. *Bioinformatics,* 34**,** 4313-4314.
1120 Christou, M., T. W. K. Fraser, V. Berg, E. Ropstad & J. H. Kamstra (2020) Calcium signaling as
1121 a possible mechanism behind increased locomotor response in zebrafish larvae
1122 exposed to a human relevant persistent organic pollutant mixture or PFOS. *Environ Res,*
1123 187**,** 109702.
1124 Clark, R. & T. Kupper (2005) Old meets new: the interaction between innate and adaptive
1125 immunity. *J Invest Dermatol,* 125**,** 629-37.
1126 Clayton, E. L., S. Minogue & M. G. Waugh (2013) Phosphatidylinositol 4-kinases and PI4P
1127 metabolism in the nervous system: roles in psychiatric and neurological diseases. *Mol*
1128 *Neurobiol,* 47**,** 361-72.
1129 Colwill, R. M. & R. Creton (2011) Imaging escape and avoidance behavior in zebrafish larvae.
1130 *Rev Neurosci,* 22**,** 63-73.
1131 Condomitti, G. & J. de Wit (2018) Heparan Sulfate Proteoglycans as Emerging Players in
1132 Synaptic Specificity. *Front Mol Neurosci,* 11**,** 14.
1133 Davalos, D., J. Grutzendler, G. Yang, J. V. Kim, Y. Zuo, S. Jung, D. R. Littman, M. L. Dustin &
1134 W. B. Gan (2005) ATP mediates rapid microglial response to local brain injury in vivo.
1135 *Nat Neurosci,* 8**,** 752-8.
1136 Davies, L. C., S. J. Jenkins, J. E. Allen & P. R. Taylor (2013) Tissue-resident macrophages. *Nat*
1137 *Immunol,* 14**,** 986-95.
1138 Davison, J. M., C. M. Akitake, M. G. Goll, J. M. Rhee, N. Gosse, H. Baier, M. E. Halpern, S. D.
1139 Leach & M. J. Parsons (2007) Transactivation from Gal4-VP16 transgenic insertions for
1140 tissue-specific cell labeling and ablation in zebrafish. *Dev Biol,* 304**,** 811-24.
1141 De Risi, M., M. Tufano, F. G. Alvino, M. G. Ferraro, G. Torromino, Y. Gigante, J. Monfregola, E.
1142 Marrocco, S. Pulcrano, L. Tunisi, C. Lubrano, D. Papy-Garcia, Y. Tuchman, A. Salleo, F.
1143 Santoro, G. C. Bellenchi, L. Cristino, A. Ballabio, A. Fraldi & E. De Leonibus (2021)
1144 Altered heparan sulfate metabolism during development triggers dopamine-dependent
1145 autistic-behaviours in models of lysosomal storage disorders. *Nat Commun,* 12**,** 3495.
1146 Delic, J., J. Coppey, H. Magdelenat & M. Coppey-Moisan (1991) Impossibility of acridine orange
1147 intercalation in nuclear DNA of the living cell. *Exp Cell Res,* 194**,** 147-53.
1148 DeWitt, J. C., S. J. Blossom & L. A. Schaider (2019) Exposure to per-fluoroalkyl and
1149 polyfluoroalkyl substances leads to immunotoxicity: epidemiological and toxicological
1150 evidence. *J Expo Sci Environ Epidemiol,* 29**,** 148-156.
1151 DeWitt, J. C., C. B. Copeland & R. W. Luebke (2009a) Suppression of humoral immunity by
1152 perfluorooctanoic acid is independent of elevated serum corticosterone concentration in
1153 mice. *Toxicol Sci,* 109**,** 106-12.
1154 DeWitt, J. C., M. M. Peden-Adams, J. M. Keller & D. R. Germolec (2012) Immunotoxicity of
1155 perfluorinated compounds: recent developments. *Toxicol Pathol,* 40**,** 300-11.
1156 DeWitt, J. C., A. Shnyra, M. Z. Badr, S. E. Loveless, D. Hoban, S. R. Frame, R. Cunard, S. E.
1157 Anderson, B. J. Meade, M. M. Peden-Adams, R. W. Luebke & M. I. Luster (2009b)
1158 Immunotoxicity of perfluorooctanoic acid and perfluorooctane sulfonate and the role of
1159 peroxisome proliferator-activated receptor alpha. *Crit Rev Toxicol,* 39**,** 76-94.
1160 DeWitt, J. C., W. C. Williams, N. J. Creech & R. W. Luebke (2016) Suppression of antigen-
1161 specific antibody responses in mice exposed to perfluorooctanoic acid: Role of
1162 PPARalpha and T- and B-cell targeting. *J Immunotoxicol,* 13**,** 38-45.
1163 Dissing-Olesen, L., J. M. LeDue, R. L. Rungta, J. K. Hefendehl, H. B. Choi & B. A. MacVicar
1164 (2014) Activation of neuronal NMDA receptors triggers transient ATP-mediated
1165 microglial process outgrowth. *J Neurosci,* 34**,** 10511-27.

1166 Donat, C. K., G. Scott, S. M. Gentleman & M. Sastre (2017) Microglial Activation in Traumatic
1167 Brain Injury. *Front Aging Neurosci,* 9**,** 208.
1168 Dong, G. H., Y. H. Zhang, L. Zheng, Z. F. Liang, Y. H. Jin & Q. C. He (2012) Subchronic effects
1169 of perfluorooctanesulfonate exposure on inflammation in adult male C57BL/6 mice.
1170 *Environ Toxicol,* 27**,** 285-96.
1171 Eddin, L. B., N. K. Jha, M. F. N. Meeran, K. K. Kesari, R. Beiram & S. Ojha (2021)
1172 Neuroprotective Potential of Limonene and Limonene Containing Natural Products.
1173 *Molecules,* 26.
1174 Ellett, F., L. Pase, J. W. Hayman, A. Andrianopoulos & G. J. Lieschke (2011a) mpeg1 promoter
1175 transgenes direct macrophage-lineage expression in zebrafish. *Blood,* 117**,** e49-e56.
1176 Ellett, F., L. Pase, J. W. Hayman, A. Andrianopoulos & G. J. Lieschke (2011b) mpeg1 promoter
1177 transgenes direct macrophage-lineage expression in zebrafish. *Blood,* 117.
1178 Errico, F., T. Nuzzo, M. Carella, A. Bertolino & A. Usiello (2018) The Emerging Role of Altered
1179 d-Aspartate Metabolism in Schizophrenia: New Insights From Preclinical Models and
1180 Human Studies. *Front Psychiatry,* 9**,** 559.
1181 Eyo, U. B., J. Peng, P. Swiatkowski, A. Mukherjee, A. Bispo & L. J. Wu (2014) Neuronal
1182 hyperactivity recruits microglial processes via neuronal NMDA receptors and microglial
1183 P2Y12 receptors after status epilepticus. *J Neurosci,* 34**,** 10528-40.
1184 Fei, C., J. K. McLaughlin, L. Lipworth & J. Olsen (2008) Prenatal exposure to perfluorooctanoate
1185 (PFOA) and perfluorooctanesulfonate (PFOS) and maternally reported developmental
1186 milestones in infancy. *Environ Health Perspect,* 116**,** 1391-5.
1187 Fosque, B. F., Y. Sun, H. Dana, C. T. Yang, T. Ohyama, M. R. Tadross, R. Patel, M. Zlatic, D.
1188 S. Kim, M. B. Ahrens, V. Jayaraman, L. L. Looger & E. R. Schreiter (2015) Neural
1189 circuits. Labeling of active neural circuits in vivo with designed calcium integrators.
1190 *Science,* 347**,** 755-60.
1191 Fuentes, S., P. Vicens, M. T. Colomina & J. L. Domingo (2007) Behavioral effects in adult mice
1192 exposed to perfluorooctane sulfonate (PFOS). *Toxicology,* 242**,** 123-9.
1193 Gaballah, S., A. Swank, J. R. Sobus, X. M. Howey, J. Schmid, T. Catron, J. McCord, E. Hines,
1194 M. Strynar & T. Tal (2020) Evaluation of Developmental Toxicity, Developmental
1195 Neurotoxicity, and Tissue Dose in Zebrafish Exposed to GenX and Other PFAS. *Environ*
1196 *Health Perspect,* 128**,** 47005.
1197 Ge, J., C. Wang, X. Nie, J. Yang, H. Lu, X. Song, K. Su, T. Li, J. Han, Y. Zhang, J. Mao, Y. Gu,
1198 J. Zhao, S. Jiang & Q. Wu (2016) ROS-mediated apoptosis of HAPI microglia through
1199 p53 signaling following PFOS exposure. *Environ Toxicol Pharmacol,* 46**,** 9-16.
1200 Goldfarb, S., N. Fainstein, T. Ganz, D. Vershkov, M. Lachish & T. Ben-Hur (2021) Electric
1201 neurostimulation regulates microglial activation via retinoic acid receptor alpha signaling.
1202 *Brain Behav Immun,* 96**,** 40-53.
1203 Gomis, M. I., R. Vestergren, D. Borg & I. T. Cousins (2018) Comparing the toxic potency in vivo
1204 of long-chain perfluoroalkyl acids and fluorinated alternatives. *Environ Int,* 113**,** 1-9.
1205 Gradinaru, V., F. Zhang, C. Ramakrishnan, J. Mattis, R. Prakash, I. Diester, I. Goshen, K. R.
1206 Thompson & K. Deisseroth (2010) Molecular and cellular approaches for diversifying
1207 and extending optogenetics. *Cell,* 141**,** 154-165.
1208 Grandjean, P., E. W. Andersen, E. Budtz-Jorgensen, F. Nielsen, K. Molbak, P. Weihe & C.
1209 Heilmann (2012) Serum vaccine antibody concentrations in children exposed to
1210 perfluorinated compounds. *JAMA,* 307**,** 391-7.
1211 Grandjean, P., C. Heilmann, P. Weihe, F. Nielsen, U. B. Mogensen, A. Timmermann & E.
1212 Budtz-Jorgensen (2017) Estimated exposures to perfluorinated compounds in infancy
1213 predict attenuated vaccine antibody concentrations at age 5-years. *J Immunotoxicol,* 14**,**
1214 188-195.

Hennebelle, M., R. K. Morgan, S. Sethi, Z. Zhang, H. Chen, A. C. Grodzki, P. J. Lein & A. Y. Taha (2020) Linoleic acid-derived metabolites constitute the majority of oxylipins in the rat pup brain and stimulate axonal growth in primary rat cortical neuron-glia co-cultures in a sex-dependent manner. *J Neurochem,* 152**,** 195-207.

Henstridge, C. M., M. Tzioras & R. C. Paolicelli (2019) Glial Contribution to Excitatory and Inhibitory Synapse Loss in Neurodegeneration. *Front Cell Neurosci,* 13**,** 63.

Hiragi, T., Y. Ikegaya & R. Koyama (2018) Microglia after Seizures and in Epilepsy. *Cells,* 7.

Hoffman, K., T. F. Webster, M. G. Weisskopf, J. Weinberg & V. M. Vieira (2010) Exposure to polyfluoroalkyl chemicals and attention deficit/hyperactivity disorder in U.S. children 12-15 years of age. *Environ Health Perspect,* 118**,** 1762-7.

Hoshiko, M., I. Arnoux, E. Avignone, N. Yamamoto & E. Audinat (2012) Deficiency of the microglial receptor CX3CR1 impairs postnatal functional development of thalamocortical synapses in the barrel cortex. *J Neurosci,* 32**,** 15106-11.

Huang, H., C. Huang, L. Wang, X. Ye, C. Bai, M. T. Simonich, R. L. Tanguay & Q. Dong (2010) Toxicity, uptake kinetics and behavior assessment in zebrafish embryos following exposure to perfluorooctanesulphonicacid (PFOS). *Aquat Toxicol,* 98**,** 139-47.

Hudson, A. E., C. Gollnick, J. P. Gourdine & A. A. Prinz (2015) Degradation of extracellular chondroitin sulfate delays recovery of network activity after perturbation. *J Neurophysiol,* 114**,** 1346-52.

Jantzen, C. E., K. M. Annunziato & K. R. Cooper (2016) Behavioral, morphometric, and gene expression effects in adult zebrafish (Danio rerio) embryonically exposed to PFOA, PFOS, and PFNA. *Aquat Toxicol,* 180**,** 123-130.

Johansson, N., P. Eriksson & H. Viberg (2009) Neonatal exposure to PFOS and PFOA in mice results in changes in proteins which are important for neuronal growth and synaptogenesis in the developing brain. *Toxicol Sci,* 108**,** 412-8.

Johansson, N., A. Fredriksson & P. Eriksson (2008) Neonatal exposure to perfluorooctane sulfonate (PFOS) and perfluorooctanoic acid (PFOA) causes neurobehavioural defects in adult mice. *Neurotoxicology,* 29**,** 160-9.

Kalueff, A. V. & A. M. Stewart. 2012. *Zebrafish protocols for neurobehavioral research*. New York: Humana Press.

Kannan, K., S. Corsolini, J. Falandysz, G. Fillmann, K. S. Kumar, B. G. Loganathan, M. A. Mohd, J. Olivero, N. Van Wouwe, J. H. Yang & K. M. Aldoust (2004) Perfluorooctanesulfonate and related fluorochemicals in human blood from several countries. *Environ Sci Technol,* 38**,** 4489-95.

Keil, D. E., T. Mehlmann, L. Butterworth & M. M. Peden-Adams (2008) Gestational exposure to perfluorooctane sulfonate suppresses immune function in B6C3F1 mice. *Toxicol Sci,* 103**,** 77-85.

Kettenmann, H., U. K. Hanisch, M. Noda & A. Verkhratsky (2011) Physiology of microglia. *Physiol Rev,* 91**,** 461-553.

Kim, S. Y., C. W. Chae, H. J. Lee, Y. H. Jung, G. E. Choi, J. S. Kim, J. R. Lim, J. E. Lee, J. H. Cho, H. Park, C. Park & H. J. Han (2020) Sodium butyrate inhibits high cholesterol-induced neuronal amyloidogenesis by modulating NRF2 stabilization-mediated ROS levels: involvement of NOX2 and SOD1. *Cell Death Dis,* 11**,** 469.

Kimura, Y., C. Satou & S. Higashijima (2008) V2a and V2b neurons are generated by the final divisions of pair-producing progenitors in the zebrafish spinal cord. *Development,* 135**,** 3001-5.

Kishimoto, N., K. Shimizu & K. Sawamoto (2012) Neuronal regeneration in a zebrafish model of adult brain injury. *Dis Model Mech,* 5**,** 200-9.

1263 Kobayashi, K., S. Morita, H. Sawada, T. Mizuguchi, K. Yamada, I. Nagatsu, T. Hata, Y.
1264 Watanabe, K. Fujita & T. Nagatsu (1995) Targeted disruption of the tyrosine hydroxylase
1265 locus results in severe catecholamine depletion and perinatal lethality in mice. *J Biol*
1266 *Chem,* 270**,** 27235-43.
1267 Lenters, V., N. Iszatt, J. Forns, E. Cechova, A. Kocan, J. Legler, P. Leonards, H. Stigum & M.
1268 Eggesbo (2019) Early-life exposure to persistent organic pollutants (OCPs, PBDEs,
1269 PCBs, PFASs) and attention-deficit/hyperactivity disorder: A multi-pollutant analysis of a
1270 Norwegian birth cohort. *Environ Int,* 125**,** 33-42.
1271 Liao, C. Y., X. Y. Li, B. Wu, S. Duan & G. B. Jiang (2008) Acute enhancement of synaptic
1272 transmission and chronic inhibition of synaptogenesis induced by perfluorooctane
1273 sulfonate through mediation of voltage-dependent calcium channel. *Environ Sci Technol,*
1274 42**,** 5335-41.
1275 Lien, G. W., C. C. Huang, J. S. Shiu, M. H. Chen, W. S. Hsieh, Y. L. Guo & P. C. Chen (2016)
1276 Perfluoroalkyl substances in cord blood and attention deficit/hyperactivity disorder
1277 symptoms in seven-year-old children. *Chemosphere,* 156**,** 118-127.
1278 Liew, Z., B. Ritz, O. S. von Ehrenstein, B. H. Bech, E. A. Nohr, C. Fei, R. Bossi, T. B. Henriksen,
1279 E. C. Bonefeld-Jorgensen & J. Olsen (2015) Attention deficit/hyperactivity disorder and
1280 childhood autism in association with prenatal exposure to perfluoroalkyl substances: a
1281 nested case-control study in the Danish National Birth Cohort. *Environ Health Perspect,*
1282 123**,** 367-73.
1283 Liu, J., L. P. Clark, M. J. Bechle, A. Hajat, S. Y. Kim, A. L. Robinson, L. Sheppard, A. A. Szpiro
1284 & J. D. Marshall (2021) Disparities in Air Pollution Exposure in the United States by
1285 Race/Ethnicity and Income, 1990-2010. *Environ Health Perspect,* 129**,** 127005.
1286 Liu, M., L. Jiang, M. Wen, Y. Ke, X. Tong, W. Huang & R. Chen (2020) Microglia depletion
1287 exacerbates acute seizures and hippocampal neuronal degeneration in mouse models
1288 of epilepsy. *Am J Physiol Cell Physiol,* 319**,** C605-C610.
1289 Liu, X., Y. Jin, W. Liu, F. Wang & S. Hao (2011) Possible mechanism of perfluorooctane
1290 sulfonate and perfluorooctanoate on the release of calcium ion from calcium stores in
1291 primary cultures of rat hippocampal neurons. *Toxicol In Vitro,* 25**,** 1294-301.
1292 Liu, X., W. Liu, Y. Jin, W. Yu, F. Wang & L. Liu (2010) Effect of gestational and lactational
1293 exposure to perfluorooctanesulfonate on calcium-dependent signaling molecules gene
1294 expression in rats' hippocampus. *Arch Toxicol,* 84**,** 71-9.
1295 Mancuso, R., G. Fryatt, M. Cleal, J. Obst, E. Pipi, J. Monzon-Sandoval, E. Ribe, L. Winchester,
1296 C. Webber, A. Nevado, T. Jacobs, N. Austin, C. Theunis, K. Grauwen, E. Daniela Ruiz,
1297 A. Mudher, M. Vicente-Rodriguez, C. A. Parker, C. Simmons, D. Cash, J. Richardson, N.
1298 Consortium, D. N. C. Jones, S. Lovestone, D. Gomez-Nicola & V. H. Perry (2019)
1299 CSF1R inhibitor JNJ-40346527 attenuates microglial proliferation and
1300 neurodegeneration in P301S mice. *Brain,* 142**,** 3243-3264.
1301 Marinelli, S., B. Basilico, M. C. Marrone & D. Ragozzino (2019) Microglia-neuron crosstalk:
1302 Signaling mechanism and control of synaptic transmission. *Semin Cell Dev Biol,* 94**,**
1303 138-151.
1304 Mathuru, A. S. & S. Jesuthasan (2013) The medial habenula as a regulator of anxiety in adult
1305 zebrafish. *Front Neural Circuits,* 7**,** 99.
1306 Mkrtchyan, G., V. Aleshin, Y. Parkhomenko, T. Kaehne, M. L. Di Salvo, A. Parroni, R.
1307 Contestabile, A. Vovk, L. Bettendorff & V. Bunik (2015) Molecular mechanisms of the
1308 non-coenzyme action of thiamin in brain: biochemical, structural and pathway analysis.
1309 *Sci Rep,* 5**,** 12583.
1310 Mollenhauer, M. A., S. G. Bradshaw, P. A. Fair, W. D. McGuinn & M. M. Peden-Adams (2011)
1311 Effects of perfluorooctane sulfonate (PFOS) exposure on markers of inflammation in

female B6C3F1 mice. *J Environ Sci Health A Tox Hazard Subst Environ Eng,* 46**,** 97-108.

Morland, C., A. S. Froland, M. N. Pettersen, J. Storm-Mathisen, V. Gundersen, F. Rise & B. Hassel (2018) Propionate enters GABAergic neurons, inhibits GABA transaminase, causes GABA accumulation and lethargy in a model of propionic acidemia. *Biochem J,* 475**,** 749-758.

Muller, C., R. J. Sampson & A. S. Winter (2018) Environmental Inequality: The Social Causes and Consequences of Lead Exposure. *Annual Review of Sociology,* 44**,** 263-282.

Newell, E. W. & L. C. Schlichter (2005) Integration of K+ and Cl- currents regulate steady-state and dynamic membrane potentials in cultured rat microglia. *J Physiol,* 567**,** 869-90.

Nguyen, N. H., C. Morland, S. V. Gonzalez, F. Rise, J. Storm-Mathisen, V. Gundersen & B. Hassel (2007) Propionate increases neuronal histone acetylation, but is metabolized oxidatively by glia. Relevance for propionic acidemia. *J Neurochem,* 101**,** 806-14.

Nimmerjahn, A., F. Kirchhoff & F. Helmchen (2005) Resting microglial cells are highly dynamic surveillants of brain parenchyma in vivo. *Science,* 308**,** 1314-8.

NTP. 2016. Monograph on Immunotoxicity Associated with Exposure to Perfluorooctanoic acid (PFOA) and perfluorooctane sulfonate (PFOS).

Ode, A., K. Kallen, P. Gustafsson, L. Rylander, B. A. Jonsson, P. Olofsson, S. A. Ivarsson, C. H. Lindh & A. Rignell-Hydbom (2014) Fetal exposure to perfluorinated compounds and attention deficit hyperactivity disorder in childhood. *PLoS One,* 9**,** e95891.

Oh, J., D. H. Bennett, A. M. Calafat, D. Tancredi, D. L. Roa, R. J. Schmidt, I. Hertz-Picciotto & H. M. Shin (2021) Prenatal exposure to per- and polyfluoroalkyl substances in association with autism spectrum disorder in the MARBLES study. *Environ Int,* 147**,** 106328.

Okamoto, H., M. Agetsuma & H. Aizawa (2012) Genetic dissection of the zebrafish habenula, a possible switching board for selection of behavioral strategy to cope with fear and anxiety. *Dev Neurobiol,* 72**,** 386-94.

Olloquequi, J., E. Cornejo-Cordova, E. Verdaguer, F. X. Soriano, O. Binvignat, C. Auladell & A. Camins (2018) Excitotoxicity in the pathogenesis of neurological and psychiatric disorders: Therapeutic implications. *J Psychopharmacol,* 32**,** 265-275.

Paolicelli, R. C., G. Bolasco, F. Pagani, L. Maggi, M. Scianni, P. Panzanelli, M. Giustetto, T. A. Ferreira, E. Guiducci, L. Dumas, D. Ragozzino & C. T. Gross (2011) Synaptic pruning by microglia is necessary for normal brain development. *Science,* 333**,** 1456-8.

Pardo, B., T. B. Rodrigues, L. Contreras, M. Garzon, I. Llorente-Folch, K. Kobayashi, T. Saheki, S. Cerdan & J. Satrustegui (2011) Brain glutamine synthesis requires neuronal-born aspartate as amino donor for glial glutamate formation. *J Cereb Blood Flow Metab,* 31**,** 90-101.

Parkhitko, A. A., D. Ramesh, L. Wang, D. Leshchiner, E. Filine, R. Binari, A. L. Olsen, J. M. Asara, V. Cracan, J. D. Rabinowitz, A. Brockmann & N. Perrimon (2020) Downregulation of the tyrosine degradation pathway extends Drosophila lifespan. *Elife,* 9.

Parkhurst, C. N., G. Yang, I. Ninan, J. N. Savas, J. R. Yates, 3rd, J. J. Lafaille, B. L. Hempstead, D. R. Littman & W. B. Gan (2013) Microglia promote learning-dependent synapse formation through brain-derived neurotrophic factor. *Cell,* 155**,** 1596-609.

Paul, A. G., K. C. Jones & A. J. Sweetman (2009) A first global production, emission, and environmental inventory for perfluorooctane sulfonate. *Environ Sci Technol,* 43**,** 386-92.

Peden-Adams, M. M., J. M. Keller, J. G. Eudaly, J. Berger, G. S. Gilkeson & D. E. Keil (2008) Suppression of humoral immunity in mice following exposure to perfluorooctane sulfonate. *Toxicol Sci,* 104**,** 144-54.

Pinto, B., G. Morelli, M. Rastogi, A. Savardi, A. Fumagalli, A. Petretto, M. Bartolucci, E. Varea, T. Catelani, A. Contestabile, L. E. Perlini & L. Cancedda (2020) Rescuing Over-activated Microglia Restores Cognitive Performance in Juvenile Animals of the Dp(16) Mouse Model of Down Syndrome. *Neuron,* 108**,** 887-904 e12.

Polis, B. & A. O. Samson (2020) Role of the metabolism of branched-chain amino acids in the development of Alzheimer's disease and other metabolic disorders. *Neural Regen Res,* 15**,** 1460-1470.

Post, G. B., P. D. Cohn & K. R. Cooper (2012) Perfluorooctanoic acid (PFOA), an emerging drinking water contaminant: a critical review of recent literature. *Environ Res,* 116**,** 93-117.

Qazi, M. R., J. Bogdanska, J. L. Butenhoff, B. D. Nelson, J. W. DePierre & M. Abedi-Valugerdi (2009) High-dose, short-term exposure of mice to perfluorooctanesulfonate (PFOS) or perfluorooctanoate (PFOA) affects the number of circulating neutrophils differently, but enhances the inflammatory responses of macrophages to lipopolysaccharide (LPS) in a similar fashion. *Toxicology,* 262**,** 207-14.

Raghu, P., A. Joseph, H. Krishnan, P. Singh & S. Saha (2019) Phosphoinositides: Regulators of Nervous System Function in Health and Disease. *Front Mol Neurosci,* 12**,** 208.

Randlett, O., C. L. Wee, E. A. Naumann, O. Nnaemeka, D. Schoppik, J. E. Fitzgerald, R. Portugues, A. M. Lacoste, C. Riegler, F. Engert & A. F. Schier (2015) Whole-brain activity mapping onto a zebrafish brain atlas. *Nat Methods,* 12**,** 1039-46.

Rericha, Y., D. Cao, L. Truong, M. Simonich, J. A. Field & R. L. Tanguay (2021) Behavior Effects of Structurally Diverse Per- and Polyfluoroalkyl Substances in Zebrafish. *Chem Res Toxicol,* 34**,** 1409-1416.

Richendrfer, H., S. D. Pelkowski, R. M. Colwill & R. Creton (2012) On the edge: pharmacological evidence for anxiety-related behavior in zebrafish larvae. *Behav Brain Res,* 228**,** 99-106.

Rosen, M. B., K. P. Das, J. Rooney, B. Abbott, C. Lau & J. C. Corton (2017) PPARalpha-independent transcriptional targets of perfluoroalkyl acids revealed by transcript profiling. *Toxicology,* 387**,** 95-107.

Ryu, M. H., A. Jha, O. O. Ojo, T. H. Mahood, S. Basu, K. A. Detillieux, N. Nikoobakht, C. S. Wong, M. Loewen, A. B. Becker & A. J. Halayko (2014) Chronic exposure to perfluorinated compounds: Impact on airway hyperresponsiveness and inflammation. *Am J Physiol Lung Cell Mol Physiol,* 307**,** L765-74.

Saba, F., A. Sirigu, R. Pillai, P. Caria, L. Cordeddu, G. Carta, E. Murru, V. Sogos & S. Banni (2019) Downregulation of inflammatory markers by conjugated linoleic acid isomers in human cultured astrocytes. *Nutr Neurosci,* 22**,** 207-214.

Salcedo, C., J. V. Andersen, K. T. Vinten, L. H. Pinborg, H. S. Waagepetersen, K. K. Freude & B. I. Aldana (2021) Functional Metabolic Mapping Reveals Highly Active Branched-Chain Amino Acid Metabolism in Human Astrocytes, Which Is Impaired in iPSC-Derived Astrocytes in Alzheimer's Disease. *Front Aging Neurosci,* 13**,** 736580.

Sant, K. E., H. M. Jacobs, K. A. Borofski, J. B. Moss & A. R. Timme-Laragy (2017) Embryonic exposures to perfluorooctanesulfonic acid (PFOS) disrupt pancreatic organogenesis in the zebrafish, Danio rerio. *Environ Pollut,* 220**,** 807-817.

Sato, I., K. Kawamoto, Y. Nishikawa, S. Tsuda, M. Yoshida, K. Yaegashi, N. Saito, W. Liu & Y. Jin (2009) Neurotoxicity of perfluorooctane sulfonate (PFOS) in rats and mice after single oral exposure. *J Toxicol Sci,* 34**,** 569-74.

Sato, T., M. Takahoko & H. Okamoto (2006) HuC:Kaede, a useful tool to label neural morphologies in networks in vivo. *Genesis,* 44**,** 136-42.

1408 Schafer, D. P., E. K. Lehrman, A. G. Kautzman, R. Koyama, A. R. Mardinly, R. Yamasaki, R. M.
1409 Ransohoff, M. E. Greenberg, B. A. Barres & B. Stevens (2012) Microglia sculpt postnatal
1410 neural circuits in an activity and complement-dependent manner. *Neuron,* 74**,** 691-705.
1411 Schmidt, R., T. Beil, U. Strahle & S. Rastegar (2014) Stab wound injury of the zebrafish adult
1412 telencephalon: a method to investigate vertebrate brain neurogenesis and regeneration.
1413 *J Vis Exp***,** e51753.
1414 Schousboe, A., S. Scafidi, L. K. Bak, H. S. Waagepetersen & M. C. McKenna (2014) Glutamate
1415 metabolism in the brain focusing on astrocytes. *Adv Neurobiol,* 11**,** 13-30.
1416 Shiau, C. E., Z. Kaufman, A. M. Meireles & W. S. Talbot (2015) Differential requirement for irf8
1417 in formation of embryonic and adult macrophages in zebrafish. *PLoS One,* 10**,**
1418 e0117513.
1419 Shin, H. M., D. H. Bennett, A. M. Calafat, D. Tancredi & I. Hertz-Picciotto (2020) Modeled
1420 prenatal exposure to per- and polyfluoroalkyl substances in association with child autism
1421 spectrum disorder: A case-control study. *Environ Res,* 186**,** 109514.
1422 Sieger, D., C. Moritz, T. Ziegenhals, S. Prykhozhij & F. Peri (2012) Long-range Ca2+ waves
1423 transmit brain-damage signals to microglia. *Dev Cell,* 22**,** 1138-48.
1424 Silva, N. J., L. C. Dorman, I. D. Vainchtein, N. C. Horneck & A. V. Molofsky (2021) In situ and
1425 transcriptomic identification of microglia in synapse-rich regions of the developing
1426 zebrafish brain. *Nat Commun,* 12**,** 5916.
1427 Skogheim, T. S., K. V. F. Weyde, H. Aase, S. M. Engel, P. Suren, M. G. Oie, G. Biele, T.
1428 Reichborn-Kjennerud, A. L. Brantsaeter, L. S. Haug, A. Sabaredzovic, B. Auyeung & G.
1429 D. Villanger (2021) Prenatal exposure to per- and polyfluoroalkyl substances (PFAS)
1430 and associations with attention-deficit/hyperactivity disorder and autism spectrum
1431 disorder in children. *Environ Res,* 202**,** 111692.
1432 Spulber, S., P. Kilian, W. N. Wan Ibrahim, N. Onishchenko, M. Ulhaq, L. Norrgren, S. Negri, M.
1433 Di Tuccio & S. Ceccatelli (2014) PFOS induces behavioral alterations, including
1434 spontaneous hyperactivity that is corrected by dexamfetamine in zebrafish larvae. *PLoS*
1435 *One,* 9**,** e94227.
1436 Stein, C. R., K. J. McGovern, A. M. Pajak, P. J. Maglione & M. S. Wolff (2016) Perfluoroalkyl
1437 and polyfluoroalkyl substances and indicators of immune function in children aged 12-19
1438 y: National Health and Nutrition Examination Survey. *Pediatr Res,* 79**,** 348-57.
1439 Sunderland, E. M., X. C. Hu, C. Dassuncao, A. K. Tokranov, C. C. Wagner & J. G. Allen (2019)
1440 A review of the pathways of human exposure to poly- and perfluoroalkyl substances
1441 (PFASs) and present understanding of health effects. *J Expo Sci Environ Epidemiol,* 29**,**
1442 131-147.
1443 Szalay, G., B. Martinecz, N. Lenart, Z. Kornyei, B. Orsolits, L. Judak, E. Csaszar, R. Fekete, B.
1444 L. West, G. Katona, B. Rozsa & A. Denes (2016) Microglia protect against brain injury
1445 and their selective elimination dysregulates neuronal network activity after stroke. *Nat*
1446 *Commun,* 7**,** 11499.
1447 Szepesi, Z., O. Manouchehrian, S. Bachiller & T. Deierborg (2018) Bidirectional Microglia-
1448 Neuron Communication in Health and Disease. *Front Cell Neurosci,* 12**,** 323.
1449 Takacs, M. L. & B. D. Abbott (2007) Activation of mouse and human peroxisome proliferator-
1450 activated receptors (alpha, beta/delta, gamma) by perfluorooctanoic acid and
1451 perfluorooctane sulfonate. *Toxicol Sci,* 95**,** 108-17.
1452 Tremblay, M. E., R. L. Lowery & A. K. Majewska (2010) Microglial interactions with synapses
1453 are modulated by visual experience. *PLoS Biol,* 8**,** e1000527.
1454 Tukker, A. M., L. M. S. Bouwman, R. van Kleef, H. S. Hendriks, J. Legler & R. H. S. Westerink
1455 (2020) Perfluorooctane sulfonate (PFOS) and perfluorooctanoate (PFOA) acutely affect

human alpha1beta2gamma2L GABAA receptor and spontaneous neuronal network function in vitro. *Sci Rep,* 10**,** 5311.

Tynan, R. J., S. Naicker, M. Hinwood, E. Nalivaiko, K. M. Buller, D. V. Pow, T. A. Day & F. R. Walker (2010) Chronic stress alters the density and morphology of microglia in a subset of stress-responsive brain regions. *Brain Behav Immun,* 24**,** 1058-68.

Uppal, K., Q. A. Soltow, F. H. Strobel, W. S. Pittard, K. M. Gernert, T. Yu & D. P. Jones (2013) xMSanalyzer: automated pipeline for improved feature detection and downstream analysis of large-scale, non-targeted metabolomics data. *BMC Bioinformatics,* 14**,** 15.

Villapol, S. (2018) Roles of Peroxisome Proliferator-Activated Receptor Gamma on Brain and Peripheral Inflammation. *Cell Mol Neurobiol,* 38**,** 121-132.

Wake, H., A. J. Moorhouse, S. Jinno, S. Kohsaka & J. Nabekura (2009) Resting microglia directly monitor the functional state of synapses in vivo and determine the fate of ischemic terminals. *J Neurosci,* 29**,** 3974-80.

Wallace, C. K., L. A. Bright, J. O. Marx, R. P. Andersen, M. C. Mullins & A. J. Carty (2018) Effectiveness of Rapid Cooling as a Method of Euthanasia for Young Zebrafish (Danio rerio). *J Am Assoc Lab Anim Sci,* 57**,** 58-63.

Wang, L. Q., T. Liu, S. Yang, L. Sun, Z. Y. Zhao, L. Y. Li, Y. C. She, Y. Y. Zheng, X. Y. Ye, Q. Bao, G. H. Dong, C. W. Li & J. Cui (2021) Perfluoroalkyl substance pollutants activate the innate immune system through the AIM2 inflammasome. *Nat Commun,* 12**,** 2915.

Westerfield, M. 2000. *The zebrafish book. A guide for the laboratory use of zebrafish (Danio rerio)*. Univ. of Oregon Press, Eugene.

Xu, Y., S. Peng, X. Cao, S. Qian, S. Shen, J. Luo, X. Zhang, H. Sun, W. L. Shen, W. Jia & J. Ye (2021) High doses of butyrate induce a reversible body temperature drop through transient proton leak in mitochondria of brain neurons. *Life Sci,* 278**,** 119614.

Yu, T., Y. Park, J. M. Johnson & D. P. Jones (2009) apLCMS--adaptive processing of high-resolution LC/MS data. *Bioinformatics,* 25**,** 1930-6.

Yu, T., X. Zhang, H. Shi, J. Tian, L. Sun, X. Hu, W. Cui & D. Du (2019) P2Y12 regulates microglia activation and excitatory synaptic transmission in spinal lamina II neurons during neuropathic pain in rodents. *Cell Death Dis,* 10**,** 165.

Zeng, Z., B. Song, R. Xiao, G. Zeng, J. Gong, M. Chen, P. Xu, P. Zhang, M. Shen & H. Yi (2019) Assessing the human health risks of perfluorooctane sulfonate by in vivo and in vitro studies. *Environ Int,* 126**,** 598-610.

Zhang, L., Y. Y. Li, H. C. Zeng, M. Li, Y. J. Wan, H. J. Schluesener, Z. Y. Zhang & S. Q. Xu (2011) Perfluorooctane sulfonate induces apoptosis in N9 microglial cell line. *Int J Toxicol,* 30**,** 207-15.

Zhou, Z., N. Xu, N. Matei, D. W. McBride, Y. Ding, H. Liang, J. Tang & J. H. Zhang (2021) Sodium butyrate attenuated neuronal apoptosis via GPR41/Gbetagamma/PI3K/Akt pathway after MCAO in rats. *J Cereb Blood Flow Metab,* 41**,** 267-281.